A fully decoupled numerical method for Cahn-Hilliard-Navier-Stokes-Darcy equations based on auxiliary variable approaches

Yali Gao[a], Rui Li[b], Xiaoming He[c,*], Yanping Lin[d]

[a]*School of Mathematics and Statistics, Northwestern Polytechnical University, Xi'an Shaanxi, 710129, P.R.China*
[b]*School of Mathematics and Information Science, Shaanxi Normal University, Xi'an Shaanxi, 710119, China*
[c]*Department of Mathematics and Statistics, Missouri University of Science and Technology, Rolla, MO 65409*
[d]*Department of Applied Mathematics, The Hong Kong Polytechnic University, Hung Hom, Hong Kong*

Abstract

A fully decoupled, linearized, and unconditionally stable finite element method is developed to solve the Cahn-Hilliard-Navier-Stokes-Darcy model in the coupled free fluid region and porous medium region. By introducing two auxiliary energy variables, we derive the equivalent system that is consistent with the original system. The energy dissipation law of the proposed equivalent model is proven. To lay a solid foundation, we first present a coupled linearized time-stepping method for the reformulated system, and prove its unconditionally energy stability. In order to further improve the computational efficiency, special treatment for the interface conditions and the artificial compression approach are utilized to decouple the two subdomains and the Navier-Stokes equation. Therefore, with the discretization techniques of two existing auxiliary variable approaches, a fully decoupled and linearized numerical scheme can be developed, under the framework of a semi-implicit semi-explicit scheme for temporal discretizaion and Galerkin finite element method for spatial discretization. The grad-div stabilization is also employed to further improve the stability of auxiliary variable algorithm. The full discretization obeys the desired energy dissipation law without any temporal restriction. Moreover, the implementation process is discussed, including the adaptive mesh strategy to accurately capture the diffuse interface. Ample numerical experiments are performed to validate the typical features of developed numerical schemes, such as the accuracy, energy stability without restriction for time step size, and adaptive mesh refinement in space. Furthermore, we apply the proposed numerical method to simulate the shape relaxation and the Buoyancy-driven flows, which demonstrate the applicability of the proposed method.

Keywords: Cahn-Hilliard-Navier-Stokes-Darcy model; decoupled finite element method; auxiliary variable; artificial compression; energy stability
2020 MSC: 65M15, 65M12, 65M60, 76D05

1. Introduction

Multi-phase flow has important role in computational fluids and industrial engineering. Two-phase flow in coupled free flow region and porous medium region has become an active area due to its wide applications such as groundwater system in karst geometry [63, 74, 97], petroleum extraction in oil reservoir [4, 32, 44, 54, 55, 112, 113], industrial filtrations in biochemical field [33, 50], evaporation and condensation process in atmospheric physics [76], etc. Therefore, it is necessary to develop physically faithful models and efficient numerical algorithms to simulate the two-phase flow in free flow region and porous media.

There are several relevant models for two-phase flow in domains composed of free flow and porous media regions [16, 18, 19, 26, 46, 47, 48, 76]. Mosthaf et al. [76] proposed a computational model for two-phase porous flow coupled with single-phase free flow, which is applied to model soil evaporation in a wind field. Chen et al. [16] considered a coupled two-phase flow model for free flow overlying porous media regions cooperated with crucial interface conditions, and discussed its well-posedness. A Robin-Robin domain decomposition method was designed for this model. Diegel et al.[26] proposed a Cahn-Hilliard-Darcy-Stokes system and devised a mix finite element method for the two-phase flow. Unconditional solvability and error estimates are rigorously analysed in two and three dimensions. Han et al. [46] proposed the Cahn-Hilliard-Stokes-Darcy model with

*Corresponding author
Email addresses: gaoylimath@nwpu.edu.cn (Yali Gao), liruismis@snnu.edu.cn (Rui Li), hex@mst.edu (Xiaoming He), yanping.lin@polyu.edu.hk (Yanping Lin)

constant density and viscosity for two-phase incompressible flows in karstic geometry obeying energy dissipative law by exploiting Onsager's extremum principle, and proved its wellposedness [45, 49]. Chen et al. [19] stated a Cahn-Hilliard-Navier-Stokes-Darcy-Boussinesq system to simulate thermal convection of two-phase flow in coupled domains. Gao et al. [36] considered a Cahn-Hilliard-Navier-Stokes-Darcy model with different densities and viscosities.

The Cahn-Hilliard-Stokes-Darcy system with constant density and viscosity is proposed in [46], consisting of the Cahn-Hilliard-Stokes equation in free flow region, the Cahn-Hilliard-Darcy equation in porous media region, and seven interface conditions to couple the two-phase flow models in two subdomains [18, 20]. Partially decoupled numerical methods with energy stability are constructed for solving the Cahn-Hilliard-Stokes-Darcy model [18] and Cahn-Hilliard-Navier-Stokes-Darcy (CHNSD) model [37]. However, the velocity and pressure are still coupled in free flow region, and sequently one needs to solve the algebra system with variable coefficients. To further improve the efficiency for solving the CHNSD model, we will follow the scalar auxiliary variable approach [90, 91] to introduce auxiliary variables and design a fully decoupled, linearized and unconditional energy stable finite element method.

There are several successful techniques that can well handle the stiffness of phase field model, such as the convex-splitting strategy [8, 41, 66, 83, 89, 101], the stabilization method [35, 56, 92, 100, 109], the Invariant Energy Quadratization (IEQ) approach [62, 99, 104, 107, 111], the scalar auxiliary variable (SAV) approach [1, 34, 38, 61, 67, 82, 90, 91], generalized positive auxiliary variable (gPAV) approach [68, 69, 108], and the zero-energy-contribution approach [102, 103, 105, 106, 110, 111]. Among these options, the SAV and gPAV approaches only need the bounded below restriction of free energy. They can explicitly treat the nonlinear bulk energy by introducing scalar auxiliary variables independent of the spatial variable. Eventually the whole system can be decoupled into linear equations with constant coefficients. Hence we will utilize both of them in this paper. Furthermore, the artificial compressible (AC) method [25, 42, 51] is to relax the divergence-free constraint for incompressible fluid by adding a regularization. Hence it has been intensively applied to break the coupling between velocity and pressure in numerical procedure [57]. The artificial compressible method is closely linked to pressure correction, while the spurious pressure boundary condition is not required [80]. Inspired by these works, multiple auxiliary energy variables and artificial compressible methods shall be assembled as key ingredients of the exhibited numerical method in this paper.

The main idea of this paper is to employ efficient auxiliary variable schemes admitting fully decoupling and obeying energy dissipation, while avoiding a nonlinear system, since the CHNSD system is a highly nonlinear and multi-physics coupling system. On one hand, the auxiliary energy variables are introduced to efficiently deal with the strong nonlinearity and coupling in CHNSD model and design the semi-implicit semi-explicit temporal discretization. One efficient technique for domain decoupling between free flow and porous media flow is to deliberately conduct the discrete interface conditions. On the other hand, the tool for decoupling the velocity and pressure is to employ the artificial compressible method in Navier-Stokes equation. Furthermore, the grad-div stabilization shall be adopted to improve the stability of completely decoupled numerical algorithm. The finite element method is utilized for the spatial discretization. The spacial adaptive strategy are introduced to greatly help accelerating the computation without sacrificing the desired properties and the accuracy. Finally only several linear elliptic equations and Possion-type equations are required to be solved at each time step.

The rest of paper is organized as follows. In Section 2, the equivalent CHNSD system based on auxiliary energy variable approach is derived, the weak formulation is stated with corresponding energy dissipation that we desire to inherit for numerical schemes, and a coupled linearized time-stepping scheme is discussed. In Section 3, we propose the totally decoupled, linear full discretization scheme on the baseline of finite element discretization by exploiting artificial compression and grad-div stabilization, thereby rigorously analyze the discrete energy stability without time step restriction for fully discretization. The implementation of constructed numerical scheme is also discussed. In Section 4, ample numerical experiences are simulated to verify the effectiveness of numerical methods. Finally, we give a brief conclusion in Section 5.

2. Cahn-Hilliard-Navier-Stokes-Darcy model

In this section, we first introduce the Cahn-Hilliard-Navier-Stokes-Darcy model [37, 46] and the two auxiliary variables to derive the equivalent system. Then we provide the corresponding weak formulation, and show that the dissipative energy law is satisfied for the reformulated auxiliary variable system in the PDE level.

2.1. The original model system and the transformed equivalent system

The CHNSD model is considered on a bounded domain $\Omega = \Omega_c \bigcup \Omega_m \subset \mathbb{R}^d$ $(d = 2, 3)$ consisting of the free flow region Ω_c and the porous media region Ω_m. We assume that the boundaries of subdomains Ω_c and Ω_m,

denoted by $\partial\Omega_c$ and $\partial\Omega_m$, are Lipschitz continuous. Let the interface of coupled free flow region and porous media be $\Gamma = \partial\Omega_m \cap \partial\Omega_c$, $\boldsymbol{n}_c$ and $\boldsymbol{n}_m$ be the unit outer normal vectors to the conduit and matrix on interface Γ, respectively, and $\boldsymbol{n}_c = -\boldsymbol{n}_m$. Denote $\Gamma_m = \partial\Omega_m \backslash \Gamma$, $\Gamma_c = \partial\Omega_c \backslash \Gamma$, a typical geometry in two dimensions is illustrated in Figure 1.

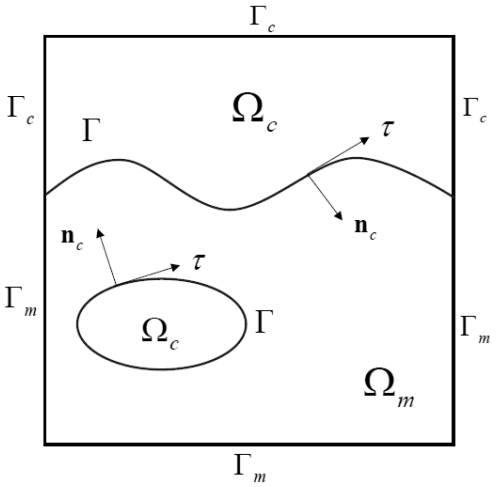

Figure 1: A sketch of the porous media domain Ω_m, free fluid domain Ω_c, and the interface Γ.

Let $f(\phi)$ be a function of phase variable ϕ such that $f(\phi) = F'(\phi)$, where $F(\phi)$ represents the Helmholtz free energy and is usually taken to be a non-convex function of ϕ. Let $\phi_j (j = c, m)$ denote the phase function to indicate the different phases for two immiscible phase flows by taking distinct value ± 1. The phase variable smoothly varies across the diffusion interface layer. The thin width of interfacial region between two-phase flow is denoted by ϵ. Let $w_j (j = c, m)$ and $M_j (j = c, m)$ denote the chemical potential and mobility related to order parameter ϕ. Variable γ represents the elastic relaxation time of mixing interface. In this paper, we consider the double-well polynomial of Ginzburg-Landau type [93]: $F(\phi) = \frac{1}{4}(\phi^2 - 1)^2$.

The two-phase flow in porous media region Ω_m is assumed to satisfy the following Cahn-Hilliard-Darcy (CHD) systems:

$$\frac{1}{\chi}\frac{\partial \boldsymbol{u}_m}{\partial t} + \mathbb{K}^{-1}\boldsymbol{u}_m = -\nabla p_m + w_m \nabla \phi_m, \tag{2.1}$$

$$\nabla \cdot \boldsymbol{u}_m = 0, \tag{2.2}$$

$$\frac{\partial \phi_m}{\partial t} + \boldsymbol{u}_m \cdot \nabla \phi_m - \nabla \cdot (M_m(\phi_m)\nabla w_m) = 0, \tag{2.3}$$

$$w_m + \gamma\epsilon\triangle\phi_m - \frac{\gamma}{\epsilon} f(\phi_m) = 0, \tag{2.4}$$

where $\boldsymbol{u}_m$ denotes the fluid discharge rate in the porous media, p_m denotes the hydraulic head. χ is the porosity of porous medium. $\mathbb{K}$ is the hydraulic conductivity tensor and has the relation $\mathbb{K} = \frac{\prod}{\nu(\phi_m)}$ with viscosity ν and permeability matrix $\prod$. In this manuscript, $\mathbb{K}$ is assumed to be a bounded, symmetric and uniformly positive definite matrix.

The two-phase flow in fluid region Ω_c is assumed to satisfy the following Cahn-Hilliard-Navier-Stokes (CHNS) systems:

$$\frac{\partial \boldsymbol{u}_c}{\partial t} + (\boldsymbol{u}_c \cdot \nabla)\boldsymbol{u}_c - \nabla \cdot \mathbb{T}(\boldsymbol{u}_c, p_c) - w_c \nabla \phi_c = 0, \tag{2.5}$$

$$\nabla \cdot \boldsymbol{u}_c = 0, \tag{2.6}$$

$$\frac{\partial \phi_c}{\partial t} + \boldsymbol{u}_c \cdot \nabla \phi_c - \nabla \cdot (M_c(\phi_c)\nabla w_c) = 0, \tag{2.7}$$

$$w_c + \gamma\epsilon\triangle\phi_c - \frac{\gamma}{\epsilon} f(\phi_c) = 0, \tag{2.8}$$

where $\mathbb{T}(\boldsymbol{u}_c, p_c) = 2\nu\mathbb{D}(u_c) - p_c\mathbb{I}$ is the stress tensor, $\mathbb{D}(u_c) = (\nabla \boldsymbol{u}_c + \nabla^T \boldsymbol{u}_c)/2$ is the deformation tensor, $\boldsymbol{u}_c$ denotes the fluid velocity, p_c denotes the kinematic pressure, ν denotes the kinematic viscosity of the fluid,

$0 < c \leq \nu$ with positive constant c.

The interface conditions on Γ connecting the CHD system and CHNS system are considered as follows [46, 49]

$$\begin{aligned}
\phi_c &= \phi_m, && (2.9)\\
w_c &= w_m, && (2.10)\\
\nabla\phi_c \cdot \boldsymbol{n}_c &= -\nabla\phi_m \cdot \boldsymbol{n}_m, && (2.11)\\
M_c(\phi_c)\nabla w_c \cdot \boldsymbol{n}_c &= -M_m(\phi_m)\nabla w_m \cdot \boldsymbol{n}_m, && (2.12)\\
\boldsymbol{u}_c \cdot \boldsymbol{n}_c &= -\boldsymbol{u}_m \cdot \boldsymbol{n}_m, && (2.13)\\
-\boldsymbol{n}_c \cdot (\mathbb{T}(\boldsymbol{u}_c, p_c) \cdot \boldsymbol{n}_c) + \frac{1}{2}|\boldsymbol{u}_c|^2 &= p_m, && (2.14)\\
-\boldsymbol{\tau}_j \cdot (\mathbb{T}(\boldsymbol{u}_c, p_c) \cdot \boldsymbol{n}_c) &= \frac{\alpha\nu\sqrt{\mathrm{d}}}{\sqrt{\mathrm{trace}(\prod)}}\boldsymbol{\tau}_j \cdot \boldsymbol{u}_c, && (2.15)
\end{aligned}$$

where $\boldsymbol{\tau}_j$ $(j = 1, \cdots, d-1)$ denote mutually orthogonal unit tangential vectors to the interface Γ. (2.9)-(2.12) describe the continuity for the phase field function, the chemical potential, and their normal derivatives. (2.13)-(2.15) can be viewed as the interface conditions of classical single-phase Stokes-Darcy model [9, 12, 13, 29, 31, 33, 65, 78, 85] or Navier-Stokes-Darcy model [7, 11, 15, 22, 30, 39, 52, 84, 95], including the mass conservation, the balance of norma force, and the so-called BJS interface condition [87]. These three interface conditions and the corresponding numerical methods to handle them with various ideas have been extensively studied and analyzed [5, 6, 10, 14, 17, 21, 27, 28, 40, 43, 53, 58, 64, 70, 73, 79, 86, 88, 98, 114].

For simplicity, the boundary conditions are considered as

$$\boldsymbol{u}_m \cdot \boldsymbol{n}_m|_{\Gamma_m} = 0, \quad \nabla\phi_m \cdot \boldsymbol{n}_m|_{\Gamma_m} = 0, \quad M_m(\phi_m)\nabla w_m \cdot \boldsymbol{n}_m|_{\Gamma_m} = 0, \tag{2.16}$$

and

$$\boldsymbol{u}_c|_{\Gamma_c} = 0, \quad \nabla\phi_c \cdot \boldsymbol{n}_c|_{\Gamma_c} = 0, \quad M_c(\phi_c)\nabla w_c \cdot \boldsymbol{n}_c|_{\Gamma_c} = 0. \tag{2.17}$$

The initial conditions are taken as

$$\phi_j(0, \boldsymbol{x}) = \phi_j^0(\boldsymbol{x}), \ j = c, m, \quad \boldsymbol{u}_c(0, \boldsymbol{x}) = \boldsymbol{u}_c^0(\boldsymbol{x}). \tag{2.18}$$

The CHNSD system (2.1)-(2.18) obeys energy dissipation associated with the following total energy law [18]

$$E(\boldsymbol{u}_m, \boldsymbol{u}_c, \phi) = \int_{\Omega_m} \frac{1}{2\chi}|\boldsymbol{u}_m|^2 \mathrm{d}\boldsymbol{x} + \int_{\Omega_c} \frac{1}{2}|\boldsymbol{u}_c|^2 \mathrm{d}\boldsymbol{x} + \gamma \int_{\Omega} \left(\frac{\epsilon}{2}|\nabla\phi|^2 + \frac{1}{\epsilon}F(\phi) \right) \mathrm{d}\boldsymbol{x}. \tag{2.19}$$

Now two new auxiliary variables are introduced for the kinetic energy and free energy as follows

$$R(t) = \sqrt{E_1(t)}, \quad U = \sqrt{\int_{\Omega} F(\phi)\mathrm{d}\boldsymbol{x} + B}, \tag{2.20}$$

where $E_1 = \int_{\Omega_m} \frac{1}{2\chi}|\boldsymbol{u}_m|^2 \mathrm{d}\boldsymbol{x} + \int_{\Omega_c} \frac{1}{2}|\boldsymbol{u}_c|^2 \mathrm{d}\boldsymbol{x}$, $\xi = \frac{R(t)}{\sqrt{E_1(t)}}$, $H(\phi) := \frac{\delta U}{\delta \phi} = \frac{f(\phi)}{\sqrt{\int_{\Omega} F(\phi)\mathrm{d}\boldsymbol{x} + B}}$, and B is a non-negative parameter. The introduction of the auxiliary variables R and U is the SAV method, which is efficient for treating nonlinear terms explicitly in energy potential by introducing scalar auxiliary variables. We reformulate

the system (2.1)-(2.8) into the following equivalent form

$$\frac{\partial \phi}{\partial t}+\xi \boldsymbol{u}\cdot\nabla\phi-\nabla\cdot(M(\phi)\nabla w)=0, \tag{2.21}$$

$$w+\gamma\epsilon\triangle\phi-\frac{\gamma}{\epsilon}H(\phi)U=0, \tag{2.22}$$

$$\frac{1}{\chi}\frac{\partial \boldsymbol{u}_m}{\partial t}+\mathbb{K}^{-1}\boldsymbol{u}_m=-\nabla p_m+\xi w_m\nabla\phi_m, \tag{2.23}$$

$$\nabla\cdot\boldsymbol{u}_m=0, \tag{2.24}$$

$$\frac{\partial \boldsymbol{u}_c}{\partial t}+\xi(\boldsymbol{u}_c\cdot\nabla)\boldsymbol{u}_c-\nabla\cdot\mathbb{T}(\boldsymbol{u}_c,p_c)-\xi w_c\nabla\phi_c=0, \tag{2.25}$$

$$\nabla\cdot\boldsymbol{u}_c=0, \tag{2.26}$$

$$\begin{aligned}2R\frac{dR}{dt}=&\int_{\Omega_c}\boldsymbol{u}_c\frac{\partial \boldsymbol{u}_c}{\partial t}\mathrm{d}\boldsymbol{x}+\frac{1}{\chi}\int_{\Omega_m}\boldsymbol{u}_m\frac{\partial \boldsymbol{u}_m}{\partial t}\mathrm{d}\boldsymbol{x}+\int_{\Omega_c}\xi(\boldsymbol{u}_c\cdot\nabla)\boldsymbol{u}_c\boldsymbol{u}_c+\frac{\xi}{2}\left(\nabla\cdot\boldsymbol{u}_c\right)\boldsymbol{u}_c\boldsymbol{u}_c\mathrm{d}\boldsymbol{x}\\&+\xi\int_{\Omega}w(\boldsymbol{u}\cdot\nabla\phi)\mathrm{d}\boldsymbol{x}-\xi\int_{\Omega_c}(w_c\nabla\phi_c)\cdot\boldsymbol{u}_c\mathrm{d}\boldsymbol{x}-\xi\int_{\Omega_m}(w_m\nabla\phi_m)\cdot\boldsymbol{u}_m\mathrm{d}\boldsymbol{x}-\frac{\xi}{2}\int_{\Gamma}|\boldsymbol{u}_c|^2\boldsymbol{u}_c\cdot\boldsymbol{n}_c\mathrm{d}s,\end{aligned} \tag{2.27}$$

$$\frac{dU}{dt}=\frac{1}{2}\int_{\Omega}H\frac{\partial\phi}{\partial t}\mathrm{d}\boldsymbol{x}. \tag{2.28}$$

Noticing that the additional terms in the right hand of (2.27) is zero since the equality $\int_{\Omega_c}(\boldsymbol{u}_c\cdot\nabla)\boldsymbol{u}_c\boldsymbol{u}_c\mathrm{d}\boldsymbol{x}+\frac{1}{2}\int_{\Omega_c}\left(\nabla\cdot\boldsymbol{u}_c\right)\boldsymbol{u}_c\boldsymbol{u}_c\mathrm{d}\boldsymbol{x}=\frac{1}{2}\int_{\Gamma}|\boldsymbol{u}_c|^2\boldsymbol{u}_c\cdot\boldsymbol{n}_c\mathrm{d}s$ holds.

2.2. The weak formulation

In this section, the weak formulation of the CHNSD model system (2.21)-(2.28) is provided. The Sobolev spaces $H^m(\Omega)$ with the norm $\|\cdot\|_m$ and $\boldsymbol{V}=[H_0^1(\Omega)]^d=\{\boldsymbol{v}\in[H^1(\Omega)]^d:\boldsymbol{v}|_{\partial\Omega}=0\}$ are utilized throughout the paper, where m is a nonnegative integer. The L^2 and L^∞ norms are simply denoted by $\|\cdot\|$ and $\|\cdot\|_\infty$. Define the Hilbert space to be $\dot{H}^1(\Omega_j)=H^1(\Omega_j)\cap\dot{L}^2(\Omega_j)$ with inner product inner product $(u,v)_{H^1}=\int_{\Omega_j}\nabla u\cdot\nabla v\,\mathrm{d}\boldsymbol{x}$ where

$$\dot{L}^2(\Omega_j):=\{v\in L^2(\Omega_j)\ \mid\ \int_{\Omega_j}v\,\mathrm{d}\boldsymbol{x}=0\}. \tag{2.29}$$

We denoted its dual space by $(\dot{H}^1(\Omega_j))'$ for simplicity. For the coupled CHNSD system, we introduce the following basic spaces

$$\begin{aligned}&\boldsymbol{X}_c=\{\boldsymbol{v}\in[H^1(\Omega_c)]^d\ \mid\ \boldsymbol{v}=0\text{ on }\Gamma_c\},\\&\boldsymbol{X}_m=\{\boldsymbol{v}\in[H^1(\Omega_m)]^d\ \mid\ \boldsymbol{v}\cdot\boldsymbol{n}_m=0\text{ on }\Gamma_m\},\\&\boldsymbol{X}_{j,div}=\{\boldsymbol{v}\in X_j\ \mid\ \nabla\cdot\boldsymbol{v}=0\},\quad Q_j=\dot{H}^1(\Omega_j),\\&Y_j=H^1(\Omega_j),\quad Y=H^1(\Omega),\quad j=c,m.\end{aligned}$$

For the domain $\Omega_j(j=c,m)$, $(\cdot,\cdot)$ denotes the L^2 inner product on the domain Ω_j decided by the subscript of integrated functions, and $\langle\cdot,\cdot\rangle$ denotes the L^2 inner product on the interface Γ. Then we have

$$\begin{aligned}&(u_m,v_m)=\int_{\Omega_m}u_mv_m\mathrm{d}\boldsymbol{x},\quad(u_c,v_c)=\int_{\Omega_c}u_cv_c\mathrm{d}\boldsymbol{x},\quad(u,v)=\int_{\Omega_m}u_mv_m\mathrm{d}\boldsymbol{x}+\int_{\Omega_c}u_cv_c\mathrm{d}\boldsymbol{x},\\&\|u_m\|:=\left(\int_{\Omega_m}|u_m|^2\mathrm{d}\boldsymbol{x}\right)^{\frac{1}{2}},\quad\|u_c\|:=\left(\int_{\Omega_c}|u_c|^2\mathrm{d}\boldsymbol{x}\right)^{\frac{1}{2}},\quad\|u\|^2=\int_{\Omega_m}|u_m|^2\mathrm{d}\boldsymbol{x}+\int_{\Omega_c}|u_c|^2\mathrm{d}\boldsymbol{x},\end{aligned}$$

where $u_m:=u|_{\Omega_m}$ and $u_c:=u|_{\Omega_c}$. Let P_τ be the projection onto the tangent space on interface Γ, i.e. $P_\tau\boldsymbol{u}=\sum_{j=1}^{d-1}(\boldsymbol{u}\cdot\boldsymbol{\tau}_j)\boldsymbol{\tau}_j$. We also denote H' the dual space of H with the duality induced by the L^2 inner product.

By applying the seven interface conditions (2.9)-(2.15), we obtain the weak formulation of the equivalent system based on auxiliary variables for CHNSD system as follows: find

$$(\boldsymbol{u}_m,p_m,\boldsymbol{u}_c,p_c,\phi,w)\in(\boldsymbol{X}_m,Q_m,\boldsymbol{X}_c,Q_c,Y,Y)$$

such that

$$(\frac{\partial \phi}{\partial t}, \psi) + \xi(\boldsymbol{u}\cdot\nabla\phi, \psi) + (M(\phi)\nabla w, \nabla\psi) = 0,\ \forall\ \psi \in Y, \tag{2.30}$$

$$(w, \omega) - \gamma\epsilon(\nabla\phi, \nabla\omega) - \frac{\gamma}{\epsilon}(H(\phi)U, \omega) = 0,\ \forall\ \omega \in Y, \tag{2.31}$$

$$\frac{1}{\chi}(\frac{\partial \boldsymbol{u}_m}{\partial t}, \boldsymbol{v}) + \mathbb{K}^{-1}(\boldsymbol{u}_m, \boldsymbol{v}) + (\nabla p_m, \boldsymbol{v}) - \xi(w_m\nabla\phi_m, \boldsymbol{v}) = 0,\ \forall\ \boldsymbol{v} \in \boldsymbol{X}_m, \tag{2.32}$$

$$(\boldsymbol{u}_m, \nabla q) + \langle \boldsymbol{u}_c\cdot\boldsymbol{n}_c, q\rangle = 0,\ \forall\ q \in Q_m, \tag{2.33}$$

$$\begin{aligned}(\frac{\partial \boldsymbol{u}_c}{\partial t}, \boldsymbol{v}) &+ \xi\left((\boldsymbol{u}_c\cdot\nabla)\,\boldsymbol{u}_c, \boldsymbol{v}\right) + \frac{\xi}{2}\left((\nabla\cdot\boldsymbol{u}_c)\,\boldsymbol{u}_c, \boldsymbol{v}\right) + 2(\nu\mathbb{D}(\boldsymbol{u}_c), \mathbb{D}(\boldsymbol{v})) - (p_c, \nabla\cdot\boldsymbol{v}) - \xi(w_c\nabla\phi_c, \boldsymbol{v})\\ &+\langle p_m, \boldsymbol{v}\cdot\boldsymbol{n}_c\rangle + \frac{\xi}{2}\langle|\boldsymbol{u}_c|^2, \boldsymbol{v}\cdot\boldsymbol{n}_c\rangle + \frac{\alpha\nu\sqrt{\mathrm{d}}}{\sqrt{\mathrm{trace}(\prod)}}\langle P_\tau\boldsymbol{u}_c, P_\tau\boldsymbol{v}\rangle = 0,\ \forall\ \boldsymbol{v} \in \boldsymbol{X}_c,\end{aligned} \tag{2.34}$$

$$(\nabla\cdot\boldsymbol{u}_c, q) = 0,\ \forall\ q \in Q_c, \tag{2.35}$$

$$\begin{aligned}2R\frac{dR}{dt} &= (\frac{\partial \boldsymbol{u}_c}{\partial t}, \boldsymbol{u}_c) + \frac{1}{\chi}(\frac{\partial \boldsymbol{u}_m}{\partial t}, \boldsymbol{u}_m) + \xi((\boldsymbol{u}_c\cdot\nabla)\boldsymbol{u}_c, \boldsymbol{u}_c) + \xi(\boldsymbol{u}\cdot\nabla\phi, w) - \xi(w\nabla\phi, \boldsymbol{u})\\ &\quad+\frac{\xi}{2}((\nabla\cdot\boldsymbol{u}_c)\,\boldsymbol{u}_c, \boldsymbol{u}_c) - \frac{\xi}{2}\langle\boldsymbol{u}_c\cdot\boldsymbol{u}_c, \boldsymbol{u}_c\cdot\boldsymbol{n}_c\rangle,\end{aligned} \tag{2.36}$$

$$\frac{dU}{dt} = \frac{1}{2}(H, \frac{\partial\phi}{\partial t}), \tag{2.37}$$

where $t \in [0, T]$, T is a finite time, $\boldsymbol{u}_m \in L^\infty(0, T; [L^2(\Omega_m)]^d) \cap L^2(0, T; \boldsymbol{X}_m)$, $\boldsymbol{u}_c \in L^\infty(0, T; [L^2(\Omega_c)]^d) \cap L^2(0, T; \boldsymbol{X}_{c,div})$, $\frac{\partial \boldsymbol{u}_c}{\partial t} \in L^2(0, T; \boldsymbol{X}'_{c,div})$, $p_j \in L^2(0, T; Q_j)$, $j = \{c, m\}$, $\phi \in L^\infty(0, T; Y) \cap L^2(0, T; H^3(\Omega))$, $\frac{\partial\phi}{\partial t} \in L^2(0, T; Y')$, and $w \in L^2(0, T; Y)$.

The above weak formulation has a desired feature, which is to satisfy the energy dissipation law corresponding to the definition of total energy as follows:

$$\mathcal{E}(t) = |R|^2 + \frac{\gamma}{\epsilon}|U|^2 + \frac{\gamma\epsilon}{2}\|\nabla\phi\|^2. \tag{2.38}$$

Lemma 2.1. *The smooth solution $(\boldsymbol{u}_m, p_m, \boldsymbol{u}_c, p_c, \phi, R, U)$ of CHNSD system (2.30)-(2.37) obeys the following energy dissipation law:*

$$\frac{d}{dt}\mathcal{E} = -\mathcal{D}(t), \tag{2.39}$$

where $\mathcal{D}$ is given by

$$\mathcal{D}(t) = \|\sqrt{2\nu}\mathbb{D}(\boldsymbol{u}_c)\|^2 + \|\sqrt{\mathbb{K}^{-1}}\boldsymbol{u}_m\|^2 + \|\sqrt{M(\phi)}\nabla w\|^2 + \frac{\alpha\nu\sqrt{d}}{\sqrt{trace(\prod)}}\langle P_\tau\boldsymbol{u}_c, P_\tau\boldsymbol{u}_c\rangle. \tag{2.40}$$

Proof. Taking $\psi = w$ in (2.30) and $\omega = -\frac{\partial\phi}{\partial t}$ in (2.31), multiplying (2.37) by $\frac{2\gamma}{\epsilon}U$, and adding these resultants together, we obtain

$$\frac{\gamma\epsilon}{2}\frac{d}{dt}\|\nabla\phi\|^2 + \frac{\gamma}{\epsilon}\frac{d}{dt}|U|^2 + \xi(\boldsymbol{u}\cdot\nabla\phi, w) + \|\sqrt{M(\phi)}\nabla w\|^2 = 0. \tag{2.41}$$

Choosing $\boldsymbol{v} = \boldsymbol{u}_m$ and $q_m = p_m$ in (2.32) and (2.33), respectively, and taking the summation, we obtain

$$\frac{1}{\chi}(\frac{\partial \boldsymbol{u}_m}{\partial t}, \boldsymbol{u}_m) - \xi(w_m\nabla\phi_m, \boldsymbol{u}_m) + \langle\boldsymbol{u}_c\cdot\boldsymbol{n}_c, p_m\rangle + \|\sqrt{\mathbb{K}^{-1}}\boldsymbol{u}_m\|^2 = 0. \tag{2.42}$$

Take the test function $\boldsymbol{v} = \boldsymbol{u}_c$ in (2.34) and $q = q_c$ in (2.35). Then adding these result equations, we have

$$\begin{aligned}(\frac{\partial \boldsymbol{u}_c}{\partial t}, \boldsymbol{u}_c) &+ \xi\left((\boldsymbol{u}_c\cdot\nabla)\,\boldsymbol{u}_c, \boldsymbol{u}_c\right) + \frac{\xi}{2}\left((\nabla\cdot\boldsymbol{u}_c)\,\boldsymbol{u}_c, \boldsymbol{u}_c\right) - \xi(w_c\nabla\phi_c, \boldsymbol{u}_c) - \frac{\xi}{2}\langle|\boldsymbol{u}_c|^2, \boldsymbol{u}_c\cdot\boldsymbol{n}_c\rangle\\ &+\langle p_m, \boldsymbol{u}_c\cdot\boldsymbol{n}_c\rangle + \|\sqrt{2\nu}\mathbb{D}(\boldsymbol{u}_c)\|^2 + \frac{\alpha\nu\sqrt{\mathrm{d}}}{\sqrt{\mathrm{trace}(\prod)}}\langle P_\tau\boldsymbol{u}_c, P_\tau\boldsymbol{u}_c\rangle = 0.\end{aligned} \tag{2.43}$$

Summing (2.36) and the above resultants (2.41), (2.42), (2.43), and utilizing the fact $(\boldsymbol{u}\cdot\nabla\phi, w) = \int_\Omega(\boldsymbol{u}\cdot\nabla\phi)wd\boldsymbol{x} = \int_{\Omega_m}(w_m\nabla\phi_m)\cdot\boldsymbol{u}_m d\boldsymbol{x} + \int_{\Omega_c}(w_c\nabla\phi_c)\cdot\boldsymbol{u}_c d\boldsymbol{x} = (w_m\nabla\phi_m, \boldsymbol{u}_m) + (w_c\nabla\phi_c, \boldsymbol{u}_c)$, we derive the energy law (2.39), and then complete the proof of Lemma 2.1. □

2.3. Energy stable coupled linearized time-stepping method

We first construct the following coupled linearized time-stepping method, meanwhile maintaining the unconditional energy stability based on the multiple auxiliary variable approach, and prove its energy stability.

Let $0 = t_0 < t_1 < \cdots < t_M = T$ be a uniform partition of $[0, T]$ with time step size $\Delta t = t_{n+1} - t_n = \frac{T}{M}$. Now, we present the semi-discrete scheme based on the weak formulation (2.30)-(2.37): find

$$(\boldsymbol{u}_m^{n+1}, p_m^{n+1}, \boldsymbol{u}_c^{n+1}, p_c^{n+1}, \phi^{n+1}, w^{n+1}) \in (Q_m, \boldsymbol{X}_c, Q_c, Y, Y)$$

such that

$$(\frac{\phi^{n+1}-\phi^n}{\Delta t}, \psi) + \xi^{n+1}(\boldsymbol{u}^n\cdot\nabla\phi^n, \psi) + (M(\phi^n)\nabla w^{n+1}, \nabla\psi) = 0,\ \forall\ \psi\in Y, \tag{2.44}$$

$$(w^{n+1}, w) - \gamma\epsilon(\nabla\phi^{n+1}, \nabla w) - \frac{\gamma}{\epsilon}(H^n U^{n+1}, w) = 0,\ \forall\ w\in Y, \tag{2.45}$$

$$\frac{1}{\chi}(\frac{\boldsymbol{u}_m^{n+1}-\boldsymbol{u}_m^n}{\Delta t}, \boldsymbol{v}) + \mathbb{K}^{-1}(\boldsymbol{u}_m^{n+1}, \boldsymbol{v}) + (\nabla p_m^{n+1}, \boldsymbol{v}) - \xi^{n+1}(w_m^n\nabla\phi_m^n, \boldsymbol{v}) = 0,\ \forall\ \boldsymbol{v}\in\boldsymbol{X}_m, \tag{2.46}$$

$$(\boldsymbol{u}_m^{n+1}, \nabla q) + \langle \boldsymbol{u}_c^{n+1}\cdot\boldsymbol{n}_c, q\rangle = 0,\ \forall\ q\in Q_m, \tag{2.47}$$

$$\begin{aligned}(\frac{\boldsymbol{u}_c^{n+1}-\boldsymbol{u}_c^n}{\Delta t}, \boldsymbol{v}) &+ \xi^{n+1}\left((\boldsymbol{u}_c^n\cdot\nabla)\,\boldsymbol{u}_c^n, \boldsymbol{v}\right) + \frac{\xi^{n+1}}{2}\left((\nabla\cdot\boldsymbol{u}_c^n)\,\boldsymbol{u}_c^n, \boldsymbol{v}\right) + 2(\nu\mathbb{D}(\boldsymbol{u}_c^{n+1}), \mathbb{D}(\boldsymbol{v})) - (p_c^{n+1}, \nabla\cdot\boldsymbol{v})\\ &-\xi^{n+1}(w_c^n\nabla\phi_c^n, \boldsymbol{v}) - \frac{\xi^{n+1}}{2}\langle\boldsymbol{u}_c^n\cdot\boldsymbol{u}_c^n, \boldsymbol{v}\cdot\boldsymbol{n}_c\rangle + \langle p_m^{n+1}, \boldsymbol{v}\cdot\boldsymbol{n}_c\rangle\\ &+\frac{\alpha\nu\sqrt{\mathrm{d}}}{\sqrt{\mathrm{trace}(\prod)}}\langle P_\tau\boldsymbol{u}_c^{n+1}, P_\tau\boldsymbol{v}\rangle = 0,\ \forall\ \boldsymbol{v}\in\boldsymbol{X}_c,\end{aligned} \tag{2.48}$$

$$(\nabla\cdot\boldsymbol{u}_c^{n+1}, q) = 0,\ \forall\ q\in Q_c, \tag{2.49}$$

$$\begin{aligned}2R^{n+1}\frac{R^{n+1}-R^n}{\Delta t} &= (\frac{\boldsymbol{u}_c^{n+1}-\boldsymbol{u}_c^n}{\Delta t}, \boldsymbol{u}_c^{n+1}) + \frac{1}{\chi}(\frac{\boldsymbol{u}_m^{n+1}-\boldsymbol{u}_m^n}{\Delta t}, \boldsymbol{u}_m^{n+1}) + \xi^{n+1}((\boldsymbol{u}_c^n\cdot\nabla)\boldsymbol{u}_c^n, \boldsymbol{u}_c^{n+1})\\ &+\frac{\xi^{n+1}}{2}\left((\nabla\cdot\boldsymbol{u}_c^n)\,\boldsymbol{u}_c^n, \boldsymbol{u}_c^{n+1}\right) + \xi^{n+1}(\boldsymbol{u}^n\cdot\nabla\phi^n, w^{n+1}) - \xi^{n+1}(w_c^n\nabla\phi_c^n, \boldsymbol{u}_c^{n+1})\\ &-\xi^{n+1}(w_m^n\nabla\phi_m^n, \boldsymbol{u}_m^{n+1}) - \frac{\xi^{n+1}}{2}\langle\boldsymbol{u}_c^n\cdot\boldsymbol{u}_c^n, \boldsymbol{u}_c^{n+1}\cdot\boldsymbol{n}_c\rangle,\end{aligned} \tag{2.50}$$

$$\frac{U^{n+1}-U^n}{\Delta t} = \frac{1}{2}(H^n, \frac{\phi^{n+1}-\phi^n}{\Delta t}), \tag{2.51}$$

where $H^n := H(\phi^n)$, $\xi^{n+1} = \frac{R^{n+1}}{\sqrt{E^n}}$, $\boldsymbol{u}^n := \boldsymbol{u}_c^n$ if $\boldsymbol{x}\in\Omega_c$, $\boldsymbol{u}^n := \boldsymbol{u}_m^n$ if $\boldsymbol{x}\in\Omega_m$.

We now prove the energy stability as follows.

Theorem 2.1. *The scheme (2.44)-(2.51) is unconditionally energy stable, in the sense that its approximation $(\boldsymbol{u}_m^{n+1}, p_m^{n+1}, \boldsymbol{u}_c^{n+1}, p_c^{n+1}, \phi^{n+1}, R^{n+1}, U^{n+1})$ satisfies the following equality:*

$$\mathcal{E}^{n+1} - \mathcal{E}^n = -\mathcal{D}^{n+1}, \tag{2.52}$$

where the discrete energy $\mathcal{E}^n$ is defined as

$$\mathcal{E}^n = |R^n|^2 + \frac{\gamma}{\epsilon}|U^n|^2 + \frac{\gamma\epsilon}{2}\|\nabla\phi^n\|^2, \tag{2.53}$$

and the energy dissipation $\mathcal{D}^{n+1}$ is given by

$$\begin{aligned}\mathcal{D}^{n+1} &= \Delta t\|\sqrt{\mathbb{K}^{-1}}\boldsymbol{u}_m^{n+1}\|^2 + \Delta t\|\sqrt{2\nu}\mathbb{D}(\boldsymbol{u}_c^{n+1})\|^2 + \frac{\gamma\epsilon}{2}\|\nabla\phi^{n+1}-\nabla\phi^n\|^2 + |R^{n+1}-R^n|^2 + \frac{\gamma}{\epsilon}|U^{n+1}-U^n|^2\\ &+\Delta t\|\sqrt{M(\phi^n)}\nabla w^{n+1}\|^2 + \Delta t\frac{\alpha\nu\sqrt{d}}{\sqrt{trace(\prod)}}\langle P_\tau\boldsymbol{u}_c^{n+1}, P_\tau\boldsymbol{u}_c^{n+1}\rangle.\end{aligned} \tag{2.54}$$

Proof. We first consider Cahn-Hilliard part on whole domain Ω. Taking the test function $\psi = \Delta t w^{n+1}$ in (2.44) and $w = -(\phi^{n+1} - \phi^n)$ in (2.45), respectively, multiplying (3.10) by $\frac{2\gamma}{\epsilon}\Delta t U^{n+1}$, taking the summation, and utilizing the equality

$$2a(a-b) = a^2 - b^2 + (a-b)^2, \tag{2.55}$$

we obtain

$$\begin{aligned}\frac{\gamma\epsilon}{2}[\|\nabla\phi^{n+1}\|^2 - \|\nabla\phi^n\|^2] + \frac{\gamma}{\epsilon}[|U^{n+1}|^2 - |U^n|^2 + |U^{n+1}-U^n|^2] + \Delta t\xi^{n+1}(\boldsymbol{u}^n\cdot\nabla\phi^n, w^{n+1})\\ = -\frac{\gamma\epsilon}{2}\|\nabla\phi^{n+1} - \nabla\phi^n\|^2 - \Delta t\|\sqrt{M(\phi^n)}\nabla w^{n+1}\|^2.\end{aligned} \tag{2.56}$$

Next, we study the conduit part on free fluid region. Choosing $\boldsymbol{v} = \Delta t\boldsymbol{u}_c^{n+1}$ and $q = \Delta t p_c^{n+1}$ in (2.48) and (2.49), respectively, and adding the resultants, we have

$$\begin{aligned}(\boldsymbol{u}_c^{n+1} - \boldsymbol{u}_c^n, \boldsymbol{u}_c^{n+1}) + \Delta t\xi^{n+1}\left((\boldsymbol{u}_c^n\cdot\nabla)\boldsymbol{u}_c^n, \boldsymbol{u}_c^{n+1}\right) - \Delta t\xi^{n+1}(w_c^n\nabla\phi_c^n, \boldsymbol{u}_c^{n+1}) + \Delta t\|\sqrt{2\nu}\mathbb{D}(\boldsymbol{u}_c^{n+1})\|^2\\ + \frac{\Delta t\xi^{n+1}}{2}\left((\nabla\cdot\boldsymbol{u}_c^n)\boldsymbol{u}_c^n, \boldsymbol{u}_c^{n+1}\right) - \frac{\Delta t\xi^{n+1}}{2}\langle\boldsymbol{u}_c^n\cdot\boldsymbol{u}_c^n, \boldsymbol{u}_c^{n+1}\cdot\boldsymbol{n}_c\rangle\\ + \Delta t\langle p_m^{n+1}, \boldsymbol{u}_c^{n+1}\cdot\boldsymbol{n}_c\rangle + \Delta t\frac{\alpha\nu\sqrt{\mathrm{d}}}{\sqrt{\mathrm{trace}(\prod)}}\langle P_\tau\boldsymbol{u}_c^{n+1}, P_\tau\boldsymbol{u}_c^{n+1}\rangle = 0.\end{aligned} \tag{2.57}$$

Then, we consider the matrix part. We take $\boldsymbol{v} = \Delta t\boldsymbol{u}_m^{n+1}$ in (2.46) and $q = -\Delta t p_m^{n+1}$ in (2.47), and add the resultants to derive

$$\frac{1}{\chi}(\boldsymbol{u}_m^{n+1} - \boldsymbol{u}_m^n, \boldsymbol{u}_m^{n+1}) + \Delta t\|\sqrt{\mathbb{K}^{-1}}\boldsymbol{u}_m^{n+1}\|^2 - \Delta t\xi^{n+1}(w_m^n\nabla\phi_m^n, \boldsymbol{u}_m^{n+1}) - \Delta t\langle\boldsymbol{u}_c^{n+1}\cdot\boldsymbol{n}_c, p_m^{n+1}\rangle = 0. \tag{2.58}$$

Multiplying (2.50) by Δt, using (2.55), and summing over (2.56), (2.57) and (2.58), we have

$$\begin{aligned}|R^{n+1}|^2 - |R^n|^2 + \frac{\gamma}{\epsilon}[|U^{n+1}|^2 - |U^n|^2] + \frac{\gamma\epsilon}{2}[\|\nabla\phi^{n+1}\|^2 - \|\nabla\phi^n\|^2] + \Delta t\|\sqrt{\mathbb{K}^{-1}}\boldsymbol{u}_m^{n+1}\|^2 + \Delta t\|\sqrt{2\nu}\mathbb{D}(\boldsymbol{u}_c^{n+1})\|^2\\ + \frac{\gamma}{\epsilon}|U^{n+1}-U^n|^2 + |R^{n+1}-R^n|^2 + \Delta t\|\sqrt{M(\phi^n)}\nabla w^{n+1}\|^2 + \frac{\gamma\epsilon}{2}\|\nabla\phi^{n+1} - \nabla\phi^n\|^2\\ + \Delta t\frac{\alpha\nu\sqrt{\mathrm{d}}}{\sqrt{\mathrm{trace}(\prod)}}\langle P_\tau\boldsymbol{u}_c^{n+1}, P_\tau\boldsymbol{u}_c^{n+1}\rangle = 0,\end{aligned} \tag{2.59}$$

namely, (2.52) is obtained. Therefore, the conclusion of Theorem 2.1 follows. □

3. Fully decoupled numerical scheme and its implementation

In this section, we develop the fully decoupled scheme, and incorporate finite elements in spatial discretization to propose a fully discretized decopled scheme of the weak formulation (2.30)-(2.37). Then we rigorously analyze the unconditionally stability of discrete energy.

Let $\Im_h$ be a quasi-uniform regular triangular partition of domain Ω. We assume that the finite element spaces Y_h, Y_{jh}, $\boldsymbol{X}_{jh}$ and Q_{jh} are the approximation of spaces Y, Y_j, $\boldsymbol{X}_j$ and Q_j with $j = c, m$, respectively. Furthermore, we suppose that $\boldsymbol{X}_{ch} \subset \boldsymbol{X}_c$ and $Q_{ch} \subset Q_c$ satisfy an inf-sup condition for the divergence operator in the following sense: There exists a constant $C > 0$ independent of h such that the LBB condition

$$\inf_{0\neq q_h}\sup_{0\neq\boldsymbol{v}_h}\frac{(\nabla\cdot\boldsymbol{v}_h, q_h)}{\|\boldsymbol{v}_h\|_1} \geq C\|q_h\|, \ \forall\ q_h \in Q_{ch}, \boldsymbol{v}_h \in \boldsymbol{X}_{ch}$$

holds.

We first recall the following lemma for the estimate of the interface term from [75]:

Lemma 3.1. *There exists a constant C such that, for $\boldsymbol{v} \in \boldsymbol{X}_c$, $q_{mh} \in Q_{mh}$*

$$|\langle\boldsymbol{v}\cdot\boldsymbol{n}_c, q_{mh}\rangle| \leq C\|\boldsymbol{v}\|_{\boldsymbol{X}_{div}}\|\nabla q_{mh}\|, \tag{3.1}$$

where $\|\boldsymbol{v}\|^2_{\boldsymbol{X}_{div}} = \|\boldsymbol{v}\|^2 + \|\nabla\cdot\boldsymbol{v}\|^2$.

3.1. Fully decoupled energy-stable numerical scheme

The numerical complexity of CHNSD system mainly arises from its multi-domain and multi-physic coupling features. In the previous section, we adopt multiple auxiliary variable approach to treat the nonlinear energy potential, hence obtain a linear system. However, the implementation of coupled linearized scheme (2.44)-(2.51) needs expensive computational storage and cost since two domains are still coupled by the interface conditions, and the velocity and pressure are solved simultaneously in Navier-Stokes equations at each time level. On one hand, it requires us to treat the approximation of interface conditions by several techniques [3, 12, 51]. On the other hand, we employ the artificial compression method [57] by adding a perturbed term on the incompressible equations to separately study two independent subphysics problem of velocity and pressure for Navier-Stokes system. In this work, we modified the artificial compression scheme by introducing grad-div stabilization [81]. Taking into account the above insights under the framework of the reformulated system based on the auxiliary variables, we numerically treat the nonlinear bulk free energy according to the SAV approach [90, 91] and handle the trilinearity in Navier-Stokes according to gPAV approach [68, 69, 108]. Then we develop the following fully decoupled linearized stabilized algorithm for (2.30)-(2.37):

Step 1: Find $(\phi_h^{n+1}, w_h^{n+1}) \in Y_h \times Y_h$, such that

$$(\frac{\phi_h^{n+1}-\phi_h^n}{\Delta t}, \psi_h) + \xi^{n+1}(\boldsymbol{u}_h^n \cdot \nabla \phi_h^n, \psi_h) + (M(\phi_h^n)\nabla w_h^{n+1}, \nabla \psi_h) = 0, \ \forall\ \psi_h \in Y_h, \tag{3.2}$$

$$(w_h^{n+1}, \omega_h) - \gamma\epsilon(\nabla \phi_h^{n+1}, \nabla \omega_h) - \frac{\gamma}{\epsilon}(H_h^n U^{n+1}, \omega_h) - S(\phi_h^{n+1}-\phi_h^n, \omega_h) = 0, \ \forall\ \omega_h \in Y_h, \tag{3.3}$$

where $H_h^n := H(\phi_h^n)$ and $\boldsymbol{u}_h^n$ is defined as

$$\boldsymbol{u}_h^n := \begin{cases} \boldsymbol{u}_{ch}^n, & \boldsymbol{x} \in \Omega_c, \\ \boldsymbol{u}_{mh}^n, & \boldsymbol{x} \in \Omega_m. \end{cases} \tag{3.4}$$

Step 2: Find $p_{mh}^{n+1} \in Q_{mh}$, such that

$$\begin{aligned} -\Delta t\eta(\nabla p_{mh}^{n+1}, \nabla q_h) + \frac{\eta}{\chi}(\boldsymbol{u}_{mh}^n, \nabla q_h) + \Delta t\eta\xi^{n+1}(w_{mh}^n \nabla \phi_{mh}^n, \nabla q_h) - \beta\Delta t(\nabla p_{mh}^{n+1}, \nabla q_h) \\ + \langle \boldsymbol{u}_{ch}^n \cdot \boldsymbol{n}_c, q_h\rangle = 0, \ \forall\ q_h \in Q_{mh}, \end{aligned} \tag{3.5}$$

where $\eta = (\chi^{-1} + \Delta t\mathbb{K}^{-1})^{-1}$.

Step 3: Find $\boldsymbol{u}_{mh}^{n+1} \in \boldsymbol{X}_{mh}$ such that

$$\frac{1}{\chi}(\frac{\boldsymbol{u}_{mh}^{n+1}-\boldsymbol{u}_{mh}^n}{\Delta t}, \boldsymbol{v}_h) + \mathbb{K}^{-1}(\boldsymbol{u}_{mh}^{n+1}, \boldsymbol{v}_h) + (\nabla p_{mh}^{n+1}, \boldsymbol{v}_h) - \xi^{n+1}(w_{mh}^n \nabla \phi_{mh}^n, \boldsymbol{v}_h) = 0, \ \forall\ \boldsymbol{v}_h \in \boldsymbol{X}_{mh}. \tag{3.6}$$

Step 4: Find $\boldsymbol{u}_{ch}^{n+1} \in \boldsymbol{X}_{ch}$, such that

$$\begin{aligned} &(\frac{\boldsymbol{u}_{ch}^{n+1}-\boldsymbol{u}_{ch}^n}{\Delta t}, \boldsymbol{v}_h) + \xi^{n+1}\left((\boldsymbol{u}_{ch}^n \cdot \nabla)\,\boldsymbol{u}_{ch}^n, \boldsymbol{v}_h\right) + \frac{\xi^{n+1}}{2}\left((\nabla \cdot \boldsymbol{u}_{ch}^n)\,\boldsymbol{u}_{ch}^n, \boldsymbol{v}\right) + 2(\nu\mathbb{D}(\boldsymbol{u}_{ch}^{n+1}), \mathbb{D}(\boldsymbol{v}_h)) \\ &\quad + \zeta(\nabla \cdot \frac{\boldsymbol{u}_{ch}^{n+1}-\boldsymbol{u}_{ch}^n}{\Delta t}, \nabla \cdot \boldsymbol{v}_h) - \xi^{n+1}(w_{ch}^n \nabla \phi_{ch}^n, \boldsymbol{v}_h) - (2p_{ch}^n - p_{ch}^{n-1}, \nabla \cdot \boldsymbol{v}_h) + \langle p_{mh}^{n+1}, \boldsymbol{v}_h \cdot \boldsymbol{n}_c\rangle \\ &\quad - \frac{\xi^{n+1}}{2}\langle \boldsymbol{u}_{ch}^n \cdot \boldsymbol{u}_{ch}^n, \boldsymbol{v}_h \cdot \boldsymbol{n}_c\rangle + \frac{\alpha\nu\sqrt{\mathrm{d}}}{\sqrt{\mathrm{trace}(\prod)}}\langle P_\tau \boldsymbol{u}_{ch}^{n+1}, P_\tau \boldsymbol{v}_h\rangle = 0, \ \forall\ \boldsymbol{v}_h \in \boldsymbol{X}_{ch}. \end{aligned} \tag{3.7}$$

Step 5: Find $p_{ch}^{n+1} \in Q_{ch}$, such that

$$(p_{ch}^{n+1} - p_{ch}^n, q_h) = -\frac{1}{\Delta t}(\nabla \cdot \boldsymbol{u}_{ch}^{n+1}, q_h), \ \forall\ q_h \in Q_{ch}. \tag{3.8}$$

Step 6: Update R^{n+1} by

$$2R^{n+1}\frac{R^{n+1}-R^n}{\Delta t}=(\frac{\boldsymbol{u}_{ch}^{n+1}-\boldsymbol{u}_{ch}^n}{\Delta t},\boldsymbol{u}_{ch}^n)+\frac{1}{\chi}(\frac{\boldsymbol{u}_{mh}^{n+1}-\boldsymbol{u}_{mh}^n}{\Delta t},\boldsymbol{u}_{mh}^{n+1})+\xi^{n+1}((\boldsymbol{u}_{ch}^n\cdot\nabla)\boldsymbol{u}_{ch}^n,\boldsymbol{u}_{ch}^{n+1})$$
$$+\frac{\xi^{n+1}}{2}\left((\nabla\cdot\boldsymbol{u}_{ch}^n)\,\boldsymbol{u}_{ch}^n,\boldsymbol{u}_{ch}^{n+1}\right)+\xi^{n+1}(\boldsymbol{u}_h^n\cdot\nabla\phi_h^n,w_h^{n+1})-\xi^{n+1}(w_{ch}^n\nabla\phi_{ch}^n,\boldsymbol{u}_{ch}^{n+1})$$
$$-\xi^{n+1}(w_{mh}^n\nabla\phi_{mh}^n,\boldsymbol{u}_{mh}^{n+1})-\frac{\xi^{n+1}}{2}\langle\boldsymbol{u}_{ch}^n\cdot\boldsymbol{u}_{ch}^n,\boldsymbol{u}_{ch}^{n+1}\cdot\boldsymbol{n}_c\rangle. \tag{3.9}$$

Step 7: Update U^{n+1} by

$$\frac{U^{n+1}-U^n}{\Delta t}=\frac{1}{2}(H_h^n,\frac{\phi_h^{n+1}-\phi_h^n}{\Delta t}). \tag{3.10}$$

Remark 3.1. *The additional term $S(\phi_h^{n+1}-\phi_h^n)$ is the commonly used stabilization for the explicit the nonlinear term $f(\phi)$. The stabilization term $\beta\Delta t(\nabla p_{mh}^{n+1},\nabla q_h)$ is artificially added to ensure the unconditional stability for the linearized scheme (3.5). The parameter S and β depends only on the geometry of Ω.*

Remark 3.2. *The term $-\zeta\nabla(\nabla\cdot\frac{\boldsymbol{u}_{ch}^{n+1}-\boldsymbol{u}_{ch}^n}{\Delta t})$ in (3.7) is a grad-div stabilized term to ensure the stability continuity equation [81]. Thereafter, this allows us to obtain energy dissipation law under some approximate constant for ζ without restriction of time step size.*

Remark 3.3. *The motivation of numerical scheme (3.5) is from the following time stepping method*

$$\frac{1}{\chi}\frac{\boldsymbol{u}_{mh}^{n+1}-\boldsymbol{u}_{mh}^n}{\Delta t}+\mathbb{K}^{-1}\boldsymbol{u}_{mh}^{n+1}+\nabla p_{mh}^{n+1}-\xi^{n+1}w_{mh}^n\nabla\phi_{mh}^n=0, \tag{3.11}$$
$$\nabla\cdot\boldsymbol{u}_{mh}^{n+1}=0. \tag{3.12}$$

From (3.11), we immediately obtain

$$\boldsymbol{u}_{mh}^{n+1}=(\chi^{-1}+\Delta t\mathbb{K}^{-1})^{-1}[-\Delta t\nabla p_{mh}^{n+1}+\Delta t\xi^{n+1}w_{mh}^n\nabla\phi_{mh}^n+\frac{1}{\chi}\boldsymbol{u}_{mh}^n]. \tag{3.13}$$

Taking the inner product of (3.12) by $q_h\in Q_{mh}$, utilizing the Green's formula, and applying the discrete interface condition of mass conservation (2.13), we derive

$$(\boldsymbol{u}_{mh}^{n+1},\nabla q)-\beta\Delta t(\nabla p_{mh}^{n+1},\nabla q_h)+\langle\boldsymbol{u}_{ch}^n\cdot\boldsymbol{n}_c,q_h\rangle=0.$$

Then inserting (3.13) into above equation, we conclude (3.5).

Remark 3.4. *The artificial compressible technique is utilized in (3.8) for decoupling the velocity and pressure of Navier-Stokes system, which modified the incompressible equation into slight compressible equation. One can firstly compute $\boldsymbol{u}_{ch}^{n+1}$ by solving*

$$\frac{\boldsymbol{u}_{ch}^{n+1}-\boldsymbol{u}_{ch}^n}{\Delta t}+\xi^{n+1}\left(\boldsymbol{u}_{ch}^n\cdot\nabla\right)\boldsymbol{u}_{ch}^n-\nabla\cdot(2\nu\mathbb{D}(\boldsymbol{u}_{ch}^{n+1}))-\xi^{n+1}w_{ch}^n\nabla\phi_{ch}^n+\nabla(2p_{ch}^n-p_{ch}^{n-1})=0. \tag{3.14}$$

Then, p_h^{n+1} is updated by the following process

$$p_{ch}^{n+1}=p_{ch}^n-\frac{1}{\Delta t}\nabla\cdot\boldsymbol{u}_{ch}^{n+1}. \tag{3.15}$$

Remark 3.5. *It is worth noting that the above developed scheme (3.2)-(3.10) is fully decoupled and linearized numerical method for simulating CHNSD system. Indeed, (3.2)-(3.3), (3.5), (3.6), (3.7), (3.8), (3.9) and (3.10) are completely decoupled to obtain numerical approximations (ϕ_h^{n+1},w_h^{n+1}), p_{mh}^{n+1}, $\boldsymbol{u}_{mh}^{n+1}$, $\boldsymbol{u}_{ch}^{n+1}$, p_{ch}^{n+1}, R^{n+1} and U^{n+1} successively. More details of implementation shall be discussed in Section 3.2. Therefore, at each time step, one only needs to solve a sequence of small linear algebra systems which will provide high efficiency in practice simulation.*

We now proceed to prove the energy stability theorem as follows.

Theorem 3.1. *The scheme (3.2)-(3.10) is unconditionally stable, in the sense that its approximation* $(\boldsymbol{u}_{mh}^{n+1}, p_{mh}^{n+1}, \boldsymbol{u}_{ch}^{n+1}, p_{ch}^{n+1}, \phi_h^{n+1}, R^{n+1}, U^{n+1})$ *satisfies the following inequality:*

$$\mathcal{E}_h^{n+1} - \mathcal{E}_h^n \leq -\mathcal{D}_h^{n+1}, \tag{3.16}$$

where the modified discrete energy $\mathcal{E}_h^n$ *is defined as*

$$\mathcal{E}_h^n = |R^n|^2 + \frac{\gamma}{\epsilon}|U^n|^2 + \frac{\gamma\epsilon}{2}\|\nabla\phi_h^n\|^2 + \frac{\zeta}{2}\|\nabla\cdot\boldsymbol{u}_{ch}^n\|^2 + \frac{\Delta t^2}{2}\|\nabla p_{ch}^n\|^2, \tag{3.17}$$

and the energy dissipation $\mathcal{D}_h^{n+1}$ *is given by*

$$\begin{aligned}\mathcal{D}_h^{n+1} = {}& \Delta t\|\sqrt{\mathbb{K}^{-1}}\boldsymbol{u}_{mh}^{n+1}\|^2 + \Delta t\|\sqrt{2\nu}\mathbb{D}(\boldsymbol{u}_{ch}^{n+1})\|^2 + \frac{\gamma\epsilon}{2}\|\nabla\phi_h^{n+1} - \nabla\phi_h^n\|^2 + |R^{n+1} - R^n|^2 + \frac{\gamma}{\epsilon}|U^{n+1} - U^n|^2 \\ & + \frac{\Delta t^2}{2\delta}\|\nabla(p_{ch}^n - p_{ch}^{n-1})\|^2 + \Delta t\|\sqrt{M(\phi_h^n)}\nabla w_h^{n+1}\|^2 + S\Delta t\|\phi_h^{n+1} - \phi_h^n\|^2 \\ & + \Delta t\frac{\alpha\nu\sqrt{d}}{\sqrt{trace(\prod)}}\langle P_\tau\boldsymbol{u}_{ch}^{n+1}, P_\tau\boldsymbol{u}_{ch}^{n+1}\rangle.\end{aligned} \tag{3.18}$$

Proof. We firstly consider the full discretization (3.2) and (3.3) for Cahn-Hilliard equation. Taking $\psi_h = \Delta t w_h^{n+1}$ and $\omega_h = -(\phi_h^{n+1} - \phi_h^n)$ in (3.2) and (3.3), respectively, multiplying (3.10) by $\frac{2\gamma}{\epsilon}\Delta t U^{n+1}$, adding these resultants, and exploiting the equality (2.55), we derive

$$\begin{aligned}&\frac{\gamma\epsilon}{2}[\|\nabla\phi_h^{n+1}\|^2 - \|\nabla\phi_h^n\|^2] + \frac{\gamma}{\epsilon}[|U^{n+1}|^2 - |U^n|^2 + |U^{n+1} - U^n|^2] + \Delta t\xi^{n+1}(\boldsymbol{u}_h^n\cdot\nabla\phi_h^n, w_h^{n+1}) \\ &\qquad = -\frac{\gamma\epsilon}{2}\|\nabla\phi_h^{n+1} - \nabla\phi_h^n\|^2 - \Delta t\|\sqrt{M(\phi_h^n)}\nabla w_h^{n+1}\|^2 - S\Delta t\|\phi_h^{n+1} - \phi_h^n\|^2.\end{aligned} \tag{3.19}$$

Next, we consider the conduit part. Taking the test function $\boldsymbol{v}_h = \Delta t\boldsymbol{u}_{ch}^{n+1}$ in (3.7), we obtain

$$\begin{aligned}&(\boldsymbol{u}_{ch}^{n+1} - \boldsymbol{u}_{ch}^n, \boldsymbol{u}_{ch}^{n+1}) + \Delta t\xi^{n+1}\left((\boldsymbol{u}_{ch}^n\cdot\nabla)\,\boldsymbol{u}_{ch}^n, \boldsymbol{u}_{ch}^{n+1}\right) + \frac{\zeta}{2}[\|\nabla\cdot\boldsymbol{u}_{ch}^{n+1}\|^2 - \|\nabla\cdot\boldsymbol{u}_{ch}^n\|^2] + \Delta t\|\sqrt{2\nu}\mathbb{D}(\boldsymbol{u}_{ch}^{n+1})\|^2 \\ &\quad + \frac{\zeta}{2}\|\nabla\cdot(\boldsymbol{u}_{ch}^{n+1} - \boldsymbol{u}_{ch}^n)\|^2 - \Delta t\xi^{n+1}(w_{ch}^n\nabla\phi_{ch}^n, \boldsymbol{u}_{ch}^{n+1}) - \Delta t(2p_{ch}^n - p_{ch}^{n-1}, \nabla\cdot\boldsymbol{u}_{ch}^{n+1}) \\ &\quad + \frac{\Delta t\xi^{n+1}}{2}\left((\nabla\cdot\boldsymbol{u}_{ch}^n)\,\boldsymbol{u}_{ch}^n, \boldsymbol{u}_{ch}^{n+1}\right) - \frac{\Delta t\xi^{n+1}}{2}\langle\boldsymbol{u}_{ch}^n\cdot\boldsymbol{u}_{ch}^n, \boldsymbol{u}_{ch}^{n+1}\cdot\boldsymbol{n}_c\rangle \\ &\quad + \Delta t\langle p_{mh}^{n+1}, \boldsymbol{u}_{ch}^{n+1}\cdot\boldsymbol{n}_c\rangle + \Delta t\frac{\alpha\nu\sqrt{\mathrm{d}}}{\sqrt{\mathrm{trace}(\prod)}}\langle P_\tau\boldsymbol{u}_{ch}^{n+1}, P_\tau\boldsymbol{u}_{ch}^{n+1}\rangle = 0.\end{aligned} \tag{3.20}$$

Taking $q_h = \Delta t^2 p_{ch}^{n+1}$, $q_h = -\Delta t^2(p_{ch}^{n+1} - 2p_{ch}^n + p_{ch}^{n-1})$ in (3.8), respectively, using (2.55), and adding these resulting equations, we have

$$\begin{aligned}&\frac{1}{2}\Delta t^2[\|\nabla p_{ch}^{n+1}\|^2 - \|\nabla p_{ch}^n\|^2 + \|\nabla(p_{ch}^n - p_{ch}^{n-1})\|^2 - \|\nabla(p_{ch}^{n+1} - 2p_{ch}^n + p_{ch}^{n-1})\|^2] \\ &\qquad = -\Delta t(\nabla\cdot\boldsymbol{u}_{ch}^{n+1}, 2p_{ch}^n - p_{ch}^{n-1}).\end{aligned} \tag{3.21}$$

Now, we estimate the term $\|\nabla(p_{ch}^{n+1} - 2p_{ch}^n + p_{ch}^{n-1})\|^2$ on the left hand side of (3.21). Taking the difference of (3.8) at time step t^{n+1} and time step t^n to derive, for $\forall q_h \in Q_{ch}$,

$$-(\nabla(p_{ch}^{n+1} - 2p_{ch}^n + p_{ch}^{n-1}), \nabla q_h) = \frac{1}{\Delta t}(\nabla\cdot(\boldsymbol{u}_{ch}^{n+1} - \boldsymbol{u}_{ch}^n), q_h), \tag{3.22}$$

which implies

$$\frac{\Delta t^2}{2}\|\nabla(p_{ch}^{n+1} - 2p_{ch}^n + p_{ch}^{n-1})\|^2 \leq \frac{1}{2}\|\nabla\cdot(\boldsymbol{u}_{ch}^{n+1} - \boldsymbol{u}_{ch}^n)\|^2. \tag{3.23}$$

Taking the sum of (3.20), (3.21) and (3.23) leads to

$$
\begin{aligned}
(\boldsymbol{u}_{ch}^{n+1}-\boldsymbol{u}_{ch}^{n},\boldsymbol{u}_{ch}^{n+1})+\frac{\zeta}{2}[\|\nabla\cdot\boldsymbol{u}_{ch}^{n+1}\|^2-\|\nabla\cdot\boldsymbol{u}_{ch}^{n}\|^2]+\frac{\Delta t^2}{2}[\|\nabla p_{ch}^{n+1}\|^2-\|\nabla p_{ch}^{n}\|^2]+\Delta t\|\sqrt{2\nu}\mathbb{D}(\boldsymbol{u}_{ch}^{n+1})\|^2\\
+\frac{\Delta t^2}{2}\|\nabla(p_{ch}^{n}-p_{ch}^{n-1})\|^2+\frac{\zeta}{2}\|\nabla\cdot(\boldsymbol{u}_{ch}^{n+1}-\boldsymbol{u}_{ch}^{n})\|^2+\Delta t\xi^{n+1}\left((\boldsymbol{u}_{ch}^{n}\cdot\nabla)\,\boldsymbol{u}_{ch}^{n},\boldsymbol{u}_{ch}^{n+1}\right)\\
-\Delta t\xi^{n+1}(w_{ch}^{n}\nabla\phi_{ch}^{n},\boldsymbol{u}_{ch}^{n+1})+\frac{\Delta t\xi^{n+1}}{2}\left((\nabla\cdot\boldsymbol{u}_{ch}^{n})\,\boldsymbol{u}_{ch}^{n},\boldsymbol{u}_{ch}^{n+1}\right)-\frac{\Delta t\xi^{n+1}}{2}\langle\boldsymbol{u}_{ch}^{n}\cdot\boldsymbol{u}_{ch}^{n},\boldsymbol{u}_{ch}^{n+1}\cdot\boldsymbol{n}_c\rangle\\
+\Delta t\langle p_{mh}^{n+1},\boldsymbol{u}_{ch}^{n+1}\cdot\boldsymbol{n}_c\rangle+\Delta t\frac{\alpha\nu\sqrt{\mathrm{d}}}{\sqrt{\mathrm{trace}(\prod)}}\langle P_\tau\boldsymbol{u}_{ch}^{n+1},P_\tau\boldsymbol{u}_{ch}^{n+1}\rangle\le\frac{1}{2}\|\nabla\cdot(\boldsymbol{u}_{ch}^{n+1}-\boldsymbol{u}_{ch}^{n})\|^2. \quad (3.24)
\end{aligned}
$$

Then, we study the matrix part. Combined with (3.13), (3.5) can be rewritten as

$$
(\boldsymbol{u}_{mh}^{n+1},\nabla q_h)-\beta\Delta t(\nabla p_{mh}^{n+1},\nabla q_h)+\langle\boldsymbol{u}_{ch}^{n}\cdot\boldsymbol{n}_c,q_h\rangle=0. \quad (3.25)
$$

Choosing $\boldsymbol{v}_h=\Delta t\boldsymbol{u}_{mh}^{n+1}$ and $q_h=-\Delta t p_{mh}^{n+1}$ in (3.6) and (3.25), respectively, we add these two equations to obtain

$$
\begin{aligned}
\frac{1}{\chi}(\boldsymbol{u}_{mh}^{n+1}-\boldsymbol{u}_{mh}^{n},\boldsymbol{u}_{mh}^{n+1})+\beta\Delta t^2\|\nabla p_{mh}^{n+1}\|^2+\Delta t\|\sqrt{\mathbb{K}^{-1}}\boldsymbol{u}_{mh}^{n+1}\|^2-\Delta t\xi^{n+1}(w_{mh}^{n}\nabla\phi_{mh}^{n},\boldsymbol{u}_{mh}^{n+1})\\
-\Delta t\langle\boldsymbol{u}_{ch}^{n}\cdot\boldsymbol{n}_c,p_{mh}^{n+1}\rangle=0. \quad (3.26)
\end{aligned}
$$

Multiplying (3.9) by Δt and adding (3.19), (3.24) and (3.26) together, we obtain

$$
\begin{aligned}
|R^{n+1}|^2-|R^{n}|^2+\frac{\gamma}{\epsilon}[|U^{n+1}|^2-|U^{n}|^2]+\frac{\gamma\epsilon}{2}[\|\nabla\phi_h^{n+1}\|^2-\|\nabla\phi_h^{n}\|^2]+\frac{\zeta}{2}[\|\nabla\cdot\boldsymbol{u}_{ch}^{n+1}\|^2-\|\nabla\cdot\boldsymbol{u}_{ch}^{n}\|^2]\\
+\frac{\Delta t^2}{2}[\|\nabla p_{ch}^{n+1}\|^2-\|\nabla p_{ch}^{n}\|^2]+S\Delta t\|\phi_h^{n+1}-\phi_h^{n}\|^2+\Delta t\|\sqrt{\mathbb{K}^{-1}}\boldsymbol{u}_{mh}^{n+1}\|^2+\Delta t\|\sqrt{2\nu}\mathbb{D}(\boldsymbol{u}_{ch}^{n+1})\|^2\\
+\frac{\Delta t^2}{2}\|\nabla(p_{ch}^{n}-p_{ch}^{n-1})\|^2+\frac{\gamma}{\epsilon}|U^{n+1}-U^{n}|^2+|R^{n+1}-R^{n}|^2+\Delta t\|\sqrt{M(\phi_h^{n})}\nabla w_h^{n+1}\|^2\\
+\beta\Delta t\|\nabla p_{mh}^{n+1}\|^2+\frac{\gamma\epsilon}{2}\|\nabla\phi_h^{n+1}-\nabla\phi_h^{n}\|^2+\Delta t\frac{\alpha\nu\sqrt{\mathrm{d}}}{\sqrt{\mathrm{trace}(\prod)}}\langle P_\tau\boldsymbol{u}_{ch}^{n+1},P_\tau\boldsymbol{u}_{ch}^{n+1}\rangle\\
\le-\|\boldsymbol{u}_{ch}^{n+1}-\boldsymbol{u}_{ch}^{n}\|^2-\frac{\zeta-1}{2}\|\nabla\cdot(\boldsymbol{u}_{ch}^{n+1}-\boldsymbol{u}_{ch}^{n})\|^2+\Delta t\langle(\boldsymbol{u}_{ch}^{n+1}-\boldsymbol{u}_{ch}^{n})\cdot\boldsymbol{n}_c,p_{mh}^{n+1}\rangle, \quad (3.27)
\end{aligned}
$$

where (2.55) and the equality $(\boldsymbol{u}_{ch}^{n+1}-\boldsymbol{u}_{ch}^{n},\boldsymbol{u}_{ch}^{n}-\boldsymbol{u}_{ch}^{n+1})=-\|\boldsymbol{u}_{ch}^{n+1}-\boldsymbol{u}_{ch}^{n}\|^2$ are used.

In order to deal with the last term in (3.27), using Lemma 3.1, Young's inequality and the definition of norm $\|\cdot\|_{\boldsymbol{X}_{div}}^2$, i.e. $\|\boldsymbol{v}\|_{\boldsymbol{X}_{div}}^2=\|\boldsymbol{v}\|^2+\|\nabla\cdot\boldsymbol{v}\|^2$, we obtain

$$
\begin{aligned}
\Delta t|\langle(\boldsymbol{u}_{ch}^{n+1}-\boldsymbol{u}_{ch}^{n})\cdot\boldsymbol{n}_c,p_{mh}^{n+1}\rangle|&\le C\Delta t\|\boldsymbol{u}_{ch}^{n+1}-\boldsymbol{u}_{ch}^{n}\|_{\boldsymbol{X}_{div}}\|\nabla p_{mh}^{n+1}\|\\
&\le\frac{1}{8}\|\boldsymbol{u}_{ch}^{n+1}-\boldsymbol{u}_{ch}^{n}\|_{\boldsymbol{X}_{div}}^2+\tilde{C}\Delta t^2\|\nabla p_{mh}^{n+1}\|^2\\
&=\frac{1}{8}\|\boldsymbol{u}_{ch}^{n+1}-\boldsymbol{u}_{ch}^{n}\|^2+\frac{1}{8}\|\nabla\cdot(\boldsymbol{u}_{ch}^{n+1}-\boldsymbol{u}_{ch}^{n})\|^2+\tilde{C}\Delta t^2\|\nabla p_{mh}^{n+1}\|^2. \quad (3.28)
\end{aligned}
$$

Therefore, combining (3.28), the inequality (3.27) leads to

$$
\mathcal{E}^{n+1}-\mathcal{E}^{n}\le\mathcal{D}^{n+1}, \quad (3.29)
$$

if we impose $\beta\ge 2\tilde{C}$ and $\zeta\ge\frac{5}{4}$, which only depends on the geometry of Ω. This leads to the energy stability of the numerical scheme (3.2)-(3.10) and completes the proof of Theorem 3.1. □

3.2. Issues of implementation

In computation, we first denote

$$\boldsymbol{u}_{mh}^{n+1} = \boldsymbol{u}_{1mh}^{n+1} + \xi^{n+1}\boldsymbol{u}_{2mh}^{n+1}, \quad \boldsymbol{u}_{ch}^{n+1} = \boldsymbol{u}_{1ch}^{n+1} + \xi^{n+1}\boldsymbol{u}_{2ch}^{n+1}, \tag{3.30}$$

$$p_{mh}^{n+1} = p_{1mh}^{n+1} + \xi^{n+1}p_{2mh}^{n+1}, \quad p_{ch}^{n+1} = p_{1ch}^{n+1} + \xi^{n+1}p_{2ch}^{n+1}, \tag{3.31}$$

$$w_{h}^{n+1} = w_{1h}^{n+1} + \xi^{n+1}w_{2h}^{n+1}, \quad \phi_{h}^{n+1} = \phi_{1h}^{n+1} + \xi^{n+1}\phi_{2h}^{n+1}, \tag{3.32}$$

$$U^{n+1} = U_1^{n+1} + \xi^{n+1}U_2^{n+1}. \tag{3.33}$$

Substituting (3.32) and (3.33) into (3.2), (3.3) and (3.10), respectively, we obtain

$$(\frac{\phi_{1h}^{n+1}-\phi_h^n}{\Delta t}, \psi_h) + (M(\phi_h^n)\nabla w_{1h}^{n+1}, \nabla\psi_h) = 0, \ \forall\ \psi_h \in Y_h, \tag{3.34}$$

$$(w_{1h}^{n+1}, \omega_h) - \gamma\epsilon(\nabla\phi_{1h}^{n+1}, \nabla\omega_h) - \frac{\gamma}{\epsilon}(H_h^n U_1^{n+1}, \omega_h) - S(\phi_{1h}^{n+1}-\phi_h^n, \omega_h) = 0, \ \forall\ \omega_h \in Y_h, \tag{3.35}$$

$$(\frac{\phi_{2h}^{n+1}}{\Delta t}, \psi_h) + (\boldsymbol{u}_h^n\cdot\nabla\phi_h^n, \psi_h) + (M(\phi_h^n)\nabla w_{2h}^{n+1}, \nabla\psi_h) = 0, \ \forall\ \psi_h \in Y_h, \tag{3.36}$$

$$(w_{2h}^{n+1}, \omega_h) - \gamma\epsilon(\nabla\phi_{2h}^{n+1}, \nabla\omega_h) - \frac{\gamma}{\epsilon}(H_h^n U_2^{n+1}, \omega_h) - S(\phi_{2h}^{n+1}, \omega_h) = 0, \ \forall\ \omega_h \in Y_h, \tag{3.37}$$

$$\frac{U_1^{n+1}-U^n}{\Delta t} = \frac{1}{2}(H_h^n, \frac{\phi_{1h}^{n+1}-\phi_h^n}{\Delta t}), \tag{3.38}$$

$$\frac{U_2^{n+1}}{\Delta t} = \frac{1}{2}(H_h^n, \frac{\phi_{2h}^{n+1}}{\Delta t}), \tag{3.39}$$

We continue to split $(\phi_{1h}^{n+1}, \phi_{2h}^{n+1}, w_{1h}^{n+1}, w_{2h}^{n+1})$, respectively, to obtain

$$\phi_{1h}^{n+1} = \phi_{11h}^{n+1} + U_1^{n+1}\phi_{12h}^{n+1}, \quad \phi_{2h}^{n+1} = \phi_{21h}^{n+1} + U_2^{n+1}\phi_{22h}^{n+1}, \tag{3.40}$$

$$w_{1h}^{n+1} = w_{11h}^{n+1} + U_1^{n+1}w_{12h}^{n+1}, \quad w_{2h}^{n+1} = w_{21h}^{n+1} + U_2^{n+1}w_{22h}^{n+1}. \tag{3.41}$$

Replacing $(\phi_{1h}^{n+1}, \phi_{2h}^{n+1}, w_{1h}^{n+1}, w_{2h}^{n+1})$ in (3.34)-(3.39) by (3.40) and (3.41), and decomposing the derived equations according to U_1^{n+1} and U_2^{n+1}, the solution of the decoupled scheme can be obtained as follows:

Step 1: Find $(\phi_{11h}^{n+1}, w_{11h}^{n+1}) \in Y_h \times Y_h$, such that

$$(\frac{\phi_{11h}^{n+1}-\phi_h^n}{\Delta t}, \psi_h) + (M(\phi_h^n)\nabla w_{11h}^{n+1}, \nabla\psi_h) = 0, \ \forall\ \psi_h \in Y_h, \tag{3.42}$$

$$(w_{11h}^{n+1}, \omega_h) - \gamma\epsilon(\nabla\phi_{11h}^{n+1}, \nabla\omega_h) - S(\phi_{11h}^{n+1}-\phi_h^n, \omega_h) = 0, \ \forall\ \omega_h \in Y_h. \tag{3.43}$$

Find $(\phi_{12h}^{n+1}, w_{12h}^{n+1}) \in Y_h \times Y_h$, such that

$$(\frac{\phi_{12h}^{n+1}}{\Delta t}, \psi_h) + (M(\phi_h^n)\nabla w_{12h}^{n+1}, \nabla\psi_h) = 0, \ \forall\ \psi_h \in Y_h, \tag{3.44}$$

$$(w_{12h}^{n+1}, \omega_h) - \gamma\epsilon(\nabla\phi_{12h}^{n+1}, \nabla\omega_h) - \frac{\gamma}{\epsilon}(H_h^n, \omega_h) - S(\phi_{12h}^{n+1}, \omega_h) = 0, \ \forall\ \omega_h \in Y_h. \tag{3.45}$$

Find $(\phi_{21h}^{n+1}, w_{21h}^{n+1}) \in Y_h \times Y_h$, such that

$$(\frac{\phi_{21h}^{n+1}}{\Delta t}, \psi_h) + (\boldsymbol{u}_h^n\cdot\nabla\phi_h^n, \psi_h) + (M(\phi_h^n)\nabla w_{21h}^{n+1}, \nabla\psi_h) = 0, \ \forall\ \psi_h \in Y_h, \tag{3.46}$$

$$(w_{21h}^{n+1}, \omega_h) - \gamma\epsilon(\nabla\phi_{21h}^{n+1}, \nabla\omega_h) - S(\phi_{21h}^{n+1}, \omega_h) = 0, \ \forall\ \omega_h \in Y_h. \tag{3.47}$$

Find $(\phi_{22h}^{n+1}, w_{22h}^{n+1}) \in Y_h \times Y_h$, such that

$$(\frac{\phi_{22h}^{n+1}}{\Delta t}, \psi_h) + (M(\phi_h^n)\nabla w_{22h}^{n+1}, \nabla\psi_h) = 0, \ \forall\ \psi_h \in Y_h, \tag{3.48}$$

$$(w_{22h}^{n+1}, \omega_h) - \gamma\epsilon(\nabla\phi_{22h}^{n+1}, \nabla\omega_h) - \frac{\gamma}{\epsilon}(H_h^n, \omega_h) - S(\phi_{22h}^{n+1}, \omega_h) = 0, \ \forall\ \omega_h \in Y_h. \tag{3.49}$$

Step 2: Find $p_{1mh}^{n+1} \in Q_{mh}$, such that

$$-\Delta t\eta(\nabla p_{1mh}^{n+1}, \nabla q_h) + \frac{1}{\chi}\eta(\boldsymbol{u}_{mh}^n, \nabla q_h) - \beta\Delta t(\nabla p_{1mh}^{n+1}, \nabla q_h) + \langle \boldsymbol{u}_{ch}^n \cdot \boldsymbol{n}_c, q_h\rangle = 0,\ \forall\ q_h \in Q_{mh}. \tag{3.50}$$

Find $p_{2mh}^{n+1} \in Q_{mh}$, such that

$$-\Delta t\eta(\nabla p_{2mh}^{n+1}, \nabla q_h) - \beta\Delta t(\nabla p_{2mh}^{n+1}, \nabla q_h) + \Delta t\eta(w_{mh}^n \nabla \phi_{mh}^n, \nabla q_h) = 0, \quad \forall q_h \in Q_{mh}. \tag{3.51}$$

Step 3: Find $\boldsymbol{u}_{1mh}^{n+1} \in \boldsymbol{X}_{mh}$, such that

$$\frac{1}{\chi}(\frac{\boldsymbol{u}_{1mh}^{n+1} - \boldsymbol{u}_{mh}^n}{\Delta t}, \boldsymbol{v}_h) + \mathbb{K}^{-1}(\boldsymbol{u}_{1mh}^{n+1}, \boldsymbol{v}_h) + (\nabla p_{1mh}^{n+1}, \boldsymbol{v}_h) = 0,\ \forall\ \boldsymbol{v}_h \in \boldsymbol{X}_{mh}. \tag{3.52}$$

Find $\boldsymbol{u}_{2mh}^{n+1} \in \boldsymbol{X}_{mh}$, such that

$$\frac{1}{\chi}(\frac{\boldsymbol{u}_{2mh}^{n+1}}{\Delta t}, \boldsymbol{v}_h) + \mathbb{K}^{-1}(\boldsymbol{u}_{2mh}^{n+1}, \boldsymbol{v}_h) + (\nabla p_{2mh}^{n+1}, \boldsymbol{v}_h) - (w_{mh}^n \nabla \phi_{mh}^n, \boldsymbol{v}_h) = 0,\ \forall\ \boldsymbol{v}_h \in \boldsymbol{X}_{mh}. \tag{3.53}$$

Step 4: Find $\boldsymbol{u}_{1ch}^{n+1} \in \boldsymbol{X}_{ch}$, such that

$$\begin{aligned}(\frac{\boldsymbol{u}_{1ch}^{n+1} - \boldsymbol{u}_{ch}^n}{\Delta t}, \boldsymbol{v}_h) + 2(\nu\mathbb{D}(\boldsymbol{u}_{1ch}^{n+1}), \mathbb{D}(\boldsymbol{v}_h)) - (2p_{ch}^n - p_{ch}^{n-1}, \nabla\cdot\boldsymbol{v}_h) + \zeta(\nabla\cdot\frac{\boldsymbol{u}_{1ch}^{n+1} - \boldsymbol{u}_{ch}^n}{\Delta t}, \nabla\cdot\boldsymbol{v}_h)\\ +\langle p_{1mh}^{n+1}, \boldsymbol{v}_h\cdot\boldsymbol{n}_c\rangle + \frac{\alpha\nu\sqrt{\mathrm{d}}}{\sqrt{\mathrm{trace}(\prod)}}\langle P_\tau \boldsymbol{u}_{1ch}^{n+1}, P_\tau \boldsymbol{v}_h\rangle = 0,\ \forall\ \boldsymbol{v}_h \in \boldsymbol{X}_{ch}.\end{aligned} \tag{3.54}$$

Find $\boldsymbol{u}_{2ch}^{n+1} \in \boldsymbol{X}_{ch}$, such that

$$\begin{aligned}(\frac{\boldsymbol{u}_{2ch}^{n+1}}{\Delta t}, \boldsymbol{v}_h) + ((\boldsymbol{u}_{ch}^n\cdot\nabla)\,\boldsymbol{u}_{ch}^n, \boldsymbol{v}_h) + 2(\nu\mathbb{D}(\boldsymbol{u}_{2ch}^{n+1}), \mathbb{D}(\boldsymbol{v}_h)) + \zeta(\nabla\cdot\frac{\boldsymbol{u}_{2ch}^{n+1}}{\Delta t}, \nabla\cdot\boldsymbol{v}_h) - (w_{ch}^n\nabla\phi_{ch}^n, \boldsymbol{v}_h)\\ +\frac{1}{2}\left((\nabla\cdot\boldsymbol{u}_{ch}^n)\,\boldsymbol{u}_{ch}^n, \boldsymbol{v}_h\right) - \frac{1}{2}\langle \boldsymbol{u}_{ch}^n\cdot\boldsymbol{u}_{ch}^n, \boldsymbol{v}_h\cdot\boldsymbol{n}_c\rangle + \langle p_{2mh}^{n+1}, \boldsymbol{v}_h\cdot\boldsymbol{n}_c\rangle\\ +\frac{\alpha\nu\sqrt{\mathrm{d}}}{\sqrt{\mathrm{trace}(\prod)}}\langle P_\tau \boldsymbol{u}_{2ch}^{n+1}, P_\tau \boldsymbol{v}_h\rangle = 0,\ \forall\ \boldsymbol{v}_h \in \boldsymbol{X}_{ch}.\end{aligned} \tag{3.55}$$

Step 5: Find $p_{1ch}^{n+1} \in Q_{ch}$, such that

$$(p_{1ch}^{n+1}, q_h) = (p_{ch}^n, q_h) - \frac{1}{\Delta t}(\nabla\cdot\boldsymbol{u}_{1ch}^{n+1}, q),\ \forall\ q_h \in Q_{ch}. \tag{3.56}$$

Find $p_{2ch}^{n+1} \in Q_{ch}$, such that

$$(p_{2ch}^{n+1}, q_h) = -\frac{1}{\Delta t}(\nabla\cdot\boldsymbol{u}_{2ch}^{n+1}, q),\ \forall\ q_h \in Q_{ch}. \tag{3.57}$$

Step 6: Find U_1^{n+1}, such that

$$U_1^{n+1}[1 - \frac{1}{2}(H_h^n, \phi_{12h}^{n+1})] = U^n + \frac{1}{2}(H_h^n, \phi_{11h}^{n+1}) - \frac{1}{2}(H_h^n, \phi_h^n), \tag{3.58}$$

Find U_2^{n+1}, such that

$$U_2^{n+1}[1 - \frac{1}{2}(H_h^n, \phi_{22h}^{n+1})] = \frac{1}{2}(H_h^n, \phi_{21h}^{n+1}), \tag{3.59}$$

by using (3.40) in (3.38) and (3.39).

Step 7: Find ξ^{n+1}, such that

$$A(\xi^{n+1})^2 + B\xi^{n+1} + C = 0, \tag{3.60}$$

which is derive from (3.9) by plugging $\xi^{n+1} = \frac{R^{n+1}}{\sqrt{E^n}}$,

$$\begin{aligned}
A =& \frac{1}{\chi}(\boldsymbol{u}_{2mh}^{n+1}, \boldsymbol{u}_{2mh}^{n+1}) + \Delta t((\boldsymbol{u}_{ch}^{n}\cdot\nabla)\boldsymbol{u}_{ch}^{n}, \boldsymbol{u}_{2ch}^{n+1}) + \frac{\Delta t}{2}\left((\nabla\cdot\boldsymbol{u}_{ch}^{n})\,\boldsymbol{u}_{ch}^{n}, \boldsymbol{u}_{2ch}^{n+1}\right) - \frac{\Delta t}{2}\langle \boldsymbol{u}_{ch}^{n}\cdot\boldsymbol{u}_{ch}^{n}, \boldsymbol{u}_{2ch}^{n+1}\cdot\boldsymbol{n}_c\rangle \\
&+\Delta t(\boldsymbol{u}_{h}^{n}\cdot\nabla\phi_{h}^{n}, w_{2h}^{n+1}) - \Delta t(w_{ch}^{n}\nabla\phi_{ch}^{n}, \boldsymbol{u}_{2ch}^{n+1}) - \Delta t(w_{mh}^{n}\nabla\phi_{mh}^{n}, \boldsymbol{u}_{2mh}^{n+1}) - 2E^n, \\
B =& (\boldsymbol{u}_{2ch}^{n+1}, \boldsymbol{u}_{ch}^{n}) + \frac{1}{\chi}(\boldsymbol{u}_{1mh}^{n+1} - \boldsymbol{u}_{mh}^{n}, \boldsymbol{u}_{2mh}^{n+1}) + \frac{1}{\chi}(\boldsymbol{u}_{2mh}^{n+1}, \boldsymbol{u}_{1mh}^{n+1}) + \Delta t((\boldsymbol{u}_{ch}^{n}\cdot\nabla)\boldsymbol{u}_{ch}^{n}, \boldsymbol{u}_{1ch}^{n+1}) \\
&+\frac{\Delta t}{2}\left((\nabla\cdot\boldsymbol{u}_{ch}^{n})\,\boldsymbol{u}_{ch}^{n}, \boldsymbol{u}_{1ch}^{n+1}\right) - \frac{\Delta t}{2}\langle \boldsymbol{u}_{ch}^{n}\cdot\boldsymbol{u}_{ch}^{n}, \boldsymbol{u}_{1ch}^{n+1}\cdot\boldsymbol{n}_c\rangle + \Delta t(\boldsymbol{u}_{h}^{n}\cdot\nabla\phi_{h}^{n}, w_{1h}^{n+1}) \\
&-\Delta t(w_{ch}^{n}\nabla\phi_{ch}^{n}, \boldsymbol{u}_{1ch}^{n+1}) - \Delta t(w_{mh}^{n}\nabla\phi_{mh}^{n}, \boldsymbol{u}_{1mh}^{n+1}) + 2\sqrt{E^n}R^n, \\
C =& (\boldsymbol{u}_{1ch}^{n+1} - \boldsymbol{u}_{ch}^{n}, \boldsymbol{u}_{ch}^{n}) + \frac{1}{\chi}(\boldsymbol{u}_{1mh}^{n+1} - \boldsymbol{u}_{mh}^{n}, \boldsymbol{u}_{1mh}^{n+1}).
\end{aligned}$$

To summarize, the scheme can be implemented as follows:

Algorithm 1 Implementation of decoupled method

1: Solve $(\phi_{11h}^{n+1}, w_{11}^{n+1})$ from (3.42)-(3.43), $(\phi_{12h}^{n+1}, w_{12h}^{n+1})$ from (3.44)-(3.45), independently;
Solve $(\phi_{21h}^{n+1}, w_{21h}^{n+1})$ from (3.46)-(3.47), $(\phi_{22h}^{n+1}, w_{22h}^{n+1})$ from (3.48)-(3.49), independently;
Solve p_{1mh}^{n+1} from (3.50), p_{2mh}^{n+1} from (3.51), independently.

2: Solve $\boldsymbol{u}_{1mh}^{n+1}$ from (3.52), $\boldsymbol{u}_{2mh}^{n+1}$ from (3.53), independently;
Solve $\boldsymbol{u}_{1ch}^{n+1}$ from (3.54), $\boldsymbol{u}_{2ch}^{n+1}$ from (3.55), independently.

3: Solve p_{1ch}^{n+1} from (3.56), p_{2ch}^{n+1} from (3.57).

4: Update U_1^{n+1} from (3.58), U_2^{n+1} from (3.59).

5: Update $\phi_{1h}^{n+1}, \phi_{2h}^{n+1}, w_{1h}^{n+1}, w_{2h}^{n+1}$ from (3.40) and (3.41), respectively.

6: Solve ξ^{n+1} from nonlinear algebraic system (3.60) by using Newton's iteration.

7: Update $\boldsymbol{u}_{mh}^{n+1}$, $\boldsymbol{u}_{ch}^{n+1}$ p_{mh}^{n+1} and p_{ch}^{n+1} from (3.30) and (3.31);
Update w_h^{n+1}, ϕ_h^{n+1} and U^{n+1} from (3.32) and (3.33).

Remark 3.6. *The scalar variable ξ^{n+1} is solved from nonlinear algebraic equation (3.60) by using Newton's iteration method with an initial guess $\xi^{n+1} = 1$. The cost of this computation is very small and is essentially negligible compared with the total cost within a time step.*

3.3. Spatial adaptive strategy

The fully discrete scheme (3.2)-(3.10) leads to a sequence of discrete equations at each time step. As we know, for an equilibrium profile $\phi(x) = \tanh(x/(\sqrt{2}\epsilon))$, the phase function ϕ varies from -0.9 to 0.9 over a distance of about $2\sqrt{2}\tanh^{-1}(0.9)$. Therefore, if we take ϵ as $\epsilon_m = mh/[2\sqrt{2}\tanh^{-1}(0.9)]$, we have approximately mh transition layer [23, 60, 94]. This requires the fine discretization to accurately resolved. It is very costly to resolve the interface with a refine uniform grid on whole domain. In order improve the numerical accuracy of diffuse interface problem, adaptive mesh refinement are preferable to resolve the transition layer [96], namely, the locally fine mesh is utilized on interface layer, since small sizes of spatial mesh only required across the thin interface region.

Owning to the works in [72, 77], we resort an adaptive mesh strategy in this simulation with the following error estimators η_K on element K:

$$\eta_K^2 = h_K \int_K |\nabla\varphi|^2 \mathrm{d}\boldsymbol{x}, \quad \forall K \in \Im_h. \tag{3.61}$$

The efficiency of adaptive mesh strategy is shown in Example 3 of Section 4.

4. Numerical examples

In this section, we present various numerical examples to illustrate the features of proposed model and numerical methods. We first provide two examples to show the convergence accuracy and energy dissipation as presented in Theorem 3.1. Secondly, the shape relaxation is investigated. Finally, the developed numerical method is adopted to study the interaction of two bubbles under Buoyancy-driven flow in order to illustrate the applicability of the numerical method.

For the second order mixed formulation of the Cahn-Hilliard equation on the whole domain, we consider the quadratic elements. For Darcy equation on porous medium, we consider the Taylor-Hood pairs. For Navier-Stokes equation on free fluid region, we consider the celebrated Taylor-Hood elements. That is, for $\phi - w - \boldsymbol{u}_m - p_m - \boldsymbol{u}_c - p_c$, we consider the $P_2 - P_2 - \boldsymbol{P}_2 - P_1 - \boldsymbol{P}_2 - P_1$ elements. The stabilized parameters are $S = 2$, $\zeta = 5$ and $\beta = 2$ in the following numerical tests.

Example 1: Convergence and accuracy. Consider the CHNSD model problem on $\Omega = [0,1] \times [0,2]$ where porous region $\Omega_m = [0,1] \times [0,1]$ and free flow region $\Omega_c = [0,1] \times [1,2]$. Set $M_m = 1$, $\gamma = 1$, $\epsilon = 1$, $\nu = 1$, $\chi = 1$, $M_c = 1$ and $\mathbb{K} = \mathbb{I}$. The exact solutions are chosen as follows

$$\begin{cases} p_m = \phi_m = w_m = g(x)g_m(y)\cos(\pi t), \\ \boldsymbol{u}_m = \boldsymbol{u}_c = [x^2(y-1)^2, \ -\frac{2}{3}x(y-1)^3]^T \cos(\pi t), \\ p_c = \phi_c = w_c = g(x)g_c(y)\cos(\pi t), \end{cases} \tag{4.1}$$

where $g(x) = 16x^2(x-1)^2, g_m(y) = 16y^2(y-1)^2, g_c(y) = 16(y-1)^2(y-2)^2$. The boundary conditions and source terms correspond with the exact solution. We define the temporal L^2-norm errors between numerical solution v_h^n and exact solution $v(t_n)$ as $\|e\|_v = \|v_h^n - v(t_n)\|$, where $v = \boldsymbol{u}_c, \boldsymbol{u}_m, p_m, \phi$ with fixing spatial mesh size. The numerical test is carried out up to terminal time $T = 0.2$. In order to perform the convergence test of the fully decoupled numerical method, we take mesh size $h = \frac{1}{32}$ and time step size $\Delta t = 0.02/2^k$, $k = 0, 1, \ldots, 5$. The numerical errors as well as a reference line with slope 2 in the log-scale are displayed in Figure 2, which indicates that the fully decoupled numerical method can achieve the expected first order accuracy in time for variables $\boldsymbol{u}_c$, $\boldsymbol{u}_m$, p_m and ϕ.

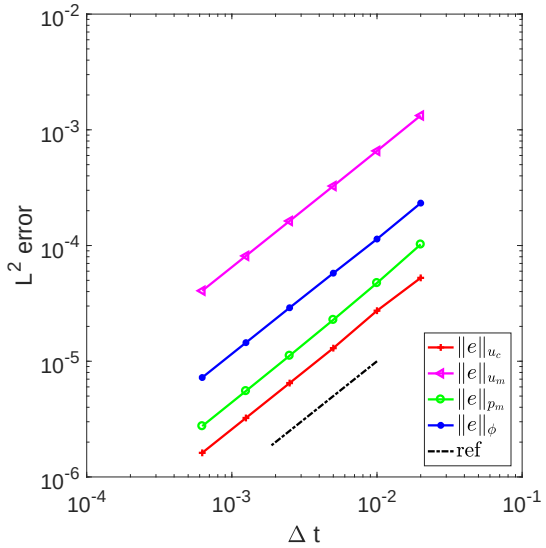

Figure 2: Log-Log plots of the L^2 error norms with different time step size Δt.

Example 2: Energy dissipation. We simulate the discrete energy dissipation with initial condition

$$\phi_0 = 0.24\cos(\pi x)\cos(2\pi y) + 0.4\cos(\pi x)\cos(3\pi y). \tag{4.2}$$

on the computational domain $\Omega = [0,1] \times [0,2]$, where $\Omega_m = [0,1] \times [0,1]$ and $\Omega_c = [0,1] \times [1,2]$. The initial velocity, pressure and chemical potential are set to zero. We choose $M = 0.01$, $\gamma = 0.01$, $\epsilon = 0.02$, $\nu = 1$,

$\frac{1}{\chi} = 0.01$, and $\mathbb{K} = 0.1\mathbb{I}$. The discrete mass $\int_\Omega \phi_h^n d\boldsymbol{x}$ and discrete energy is presented in Figure 3. From Figure 3, we can clearly observe that the discrete mass at any time level remains the initial value of mass, which illustrates the mass conservation of the proposed auxiliary variable method. The discrete energy curve of the numerical solution does decay monotonically with time, which agrees well with the theoretical result in Theorem 3.1 and validates the interface conditions (2.9)-(2.12).

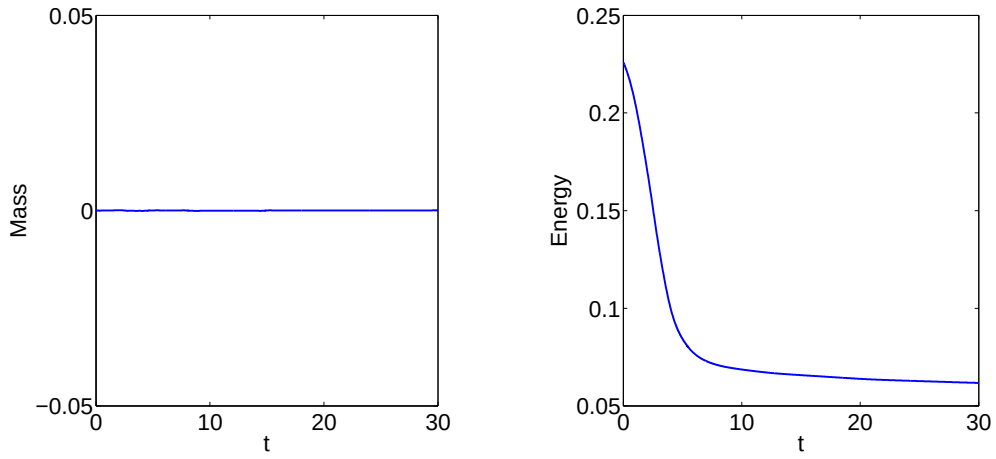

Figure 3: Evolution of discrete mass and energy.

In the following numerical experiments, adaptive mesh strategy is performed to improve the resolution of the auxiliary variable method on the fundamental mesh. The root-level mesh is taken to be uniform with $h = \frac{1}{32}$.

Example 3: Shape relaxation to a disk. We simulate the evolution of perturbed surface of the droplet in the domain $\Omega = [0,1] \times [0,2]$, where $\Omega_m = [0,1] \times [0,1]$ and $\Omega_c = [0,1] \times [1,2]$. Parameters are $M = 0.01$, $\gamma = 0.01$, $\epsilon = 0.01$, $\nu = 1$, $\frac{1}{\chi} = 0.01$, and $\mathbb{K} = 0.1\mathbb{I}$. The initial φ_0 is given in polar coordinates (r, ϖ) as follows

$$\boldsymbol{x} = (x, y) = (0.5 + r\cos(\varpi), 0.5 + r\sin(\varpi)) \quad 0 \le \varpi < 2\pi,$$

where $r = 0.25 + 0.1\cos(n\varpi)$ and n is the oscillation mode. The initial conditions for velocity, pressure and chemical potential are set to zero. The computations are performed for $n = 4$. The initial position and adaptive mesh are shown in Figure 4. Figure 5 shows the dynamic morphotype of the bubble profiles and the corresponding adaptive meshes at different time. This droplet relaxes to a desired circular shape under the effect of surface tension. Similar numerical results were also presented in [2, 59].

Figure 6 demonstrates the normalized mass, discrete total energy, and four components of total energy, namely, kinetic energy $E_{kin} = \int_{\Omega_c} \frac{1}{2}|\boldsymbol{u}_c|^2 \mathrm{d}\boldsymbol{x}$, interfacial energy $E_{inter} = \frac{\gamma\epsilon}{2}\int_\Omega |\nabla\phi|^2 \mathrm{d}\boldsymbol{x}$ and free energy of mixing $E_{mix} = \frac{\gamma}{\epsilon}\int_\Omega F(\phi)\mathrm{d}\boldsymbol{x}$ and Ginburg-Landau free energy $E_{free} = E_{inter} + E_{mix}$. In Figure 6, we normalize the discrete mass at any time level by the initial value. As graphed in Figure 6(a), the mass is conservative of the proposed numerical method. Figure 6(b) shows that the discrete energy of the numerical solution is non-increasing with time and tends to a minimum value, which illustrates the energy stability of proposed numerical algorithm. From Figure 6(c), there is a fast drop of interfacial energy and a fast increase of free energy of mixing at the beginning. The expected reasonable results verify the efficiency of developed decoupled numerical method and clearly confirm the theoretical result proven in Theorem 3.1.

The adaptive meshes on domain $[0.5, 1] \times [0.75, 1.25]$ are illustrated in Figure 7, in which the blue line represents the interface between the binary phase fluids according to -1 and 1. It is worth noting that the evolution of interface can be captured accurately. That is, the adaptive meshes are well concentrated near the interface region at each time step under the adaptive strategy discussed in the previous section.

Example 4: Buoyancy-driven flow. In this test, we study the evolution of a rising bubble in a heavier medium to illustrate the capacity of proposed numerical method for the case with different density variations. Assuming the density difference is small, we apply Boussinesq approximation [24, 71] to simulate the influence of buoyancy. We add the buoyancy-driven term $B := -\boldsymbol{g}\phi(\rho_1 - \rho_2)$ to the right side of Darcy equation (2.1) and

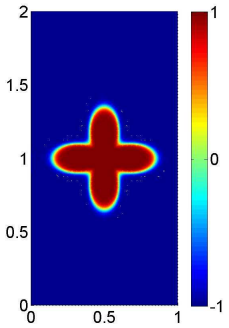

(a) Initial phase function

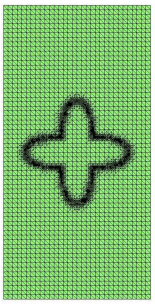

(b) Initial adaptive mesh

Figure 4: Contour plots of the initial bubble.

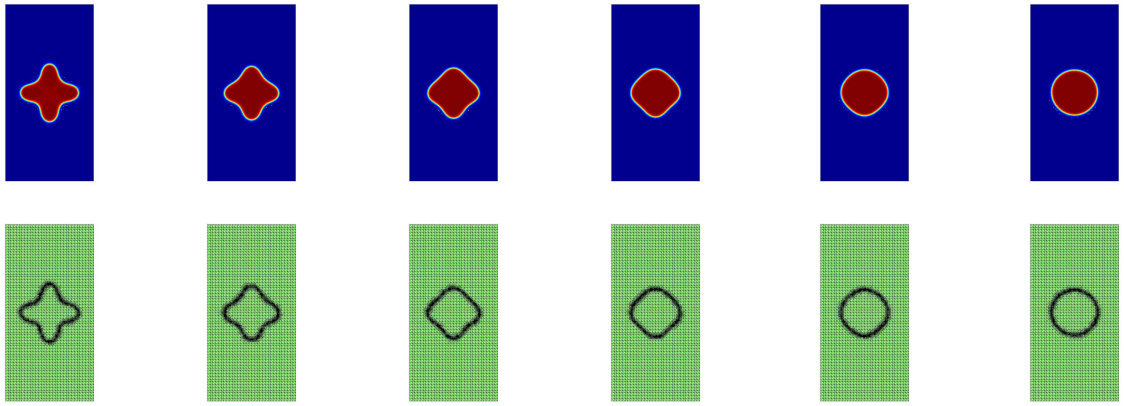

(a) $t = 0.5$ (b) $t = 1.0$ (c) $t = 1.5$ (d) $t = 2.0$ (e) $t = 3.0$ (f) $t = 5.0$

Figure 5: The evolution of a phase variable to a disk and corresponding the adaptive mesh refinement.

momentum equation (2.6) in Navier-Stokes system. Here $\rho(\phi) = \frac{\rho_1-\rho_2}{2}\phi + \frac{\rho_1+\rho_2}{2}$, ρ_1 and ρ_2 are the corresponding densities of binary fluids, and $\boldsymbol{g}$ is the gravitational acceleration with $\boldsymbol{g} = [0, g]^T$.

Choose the computational domain $\Omega = [0, 1] \times [0, 1.5]$ and the parameters $\gamma = 0.01$, $\epsilon = 0.01$, $\nu = 1$, $\mathbb{K} = 0.1\mathbb{I}$, $\rho_1 = 1$, $\rho_2 = 5$, $g = 9.8$ and $M = \sqrt{\epsilon^2 + (1-\phi)^2}$. The initial position of phase function is located as shown in the first figure of Figures 8 and 9 for horizontal and vertical rising bubbles, respectively, where the phase $\phi = 1$ represents a lighter fluid and the phase $\phi = -1$ represents a heavy fluid. The dynamics of bubbles are presented in Figures 8 and 9 under buoyancy force. From the morphotype evolution recorded in Figure 8, one can clearly observe the coalescence of two kissing bubbles and the shape deformation, eventually the rising of a single droplet across the interface between two domains. From Figure 9, we can see the deformation of two droplets due to the density different between two fluids. Then they merge into a single droplet, and gradually evolve into the stable appearance. The reasonable results illustrate the applicability of the proposed numerical scheme.

5. Conclusions

In this paper, a totally decoupled, linearized, and unconditionally stabilized auxiliary variable scheme is developed to numerically investigate the Cahn-Hilliard-Navier-Stokes-Darcy system. By introducing two scalar energy variables, the equivalent system is derived obeying corresponding energy law. We employ subtle semi-implicit approach to construct the unconditionally stable linearized numerical scheme with explicit treatment for the nonlinear terms. In order to further improve the computational efficiency, the artificial compression technique is utilized to decouple the velocity and pressure in Navier-Stokes. Meanwhile, we carefully handle the interface conditions connecting the matrix and conduits. Hence we eventually develop a fully decoupled numerical scheme. The finite element method is utilized in spacial discretization to construct the fully discrete algorithm. Moreover, the unconditional stability of numerical scheme is achieved by incorporating modular grad-div stabilization. Based on these ideas, the developed numerical scheme has several desired features, such

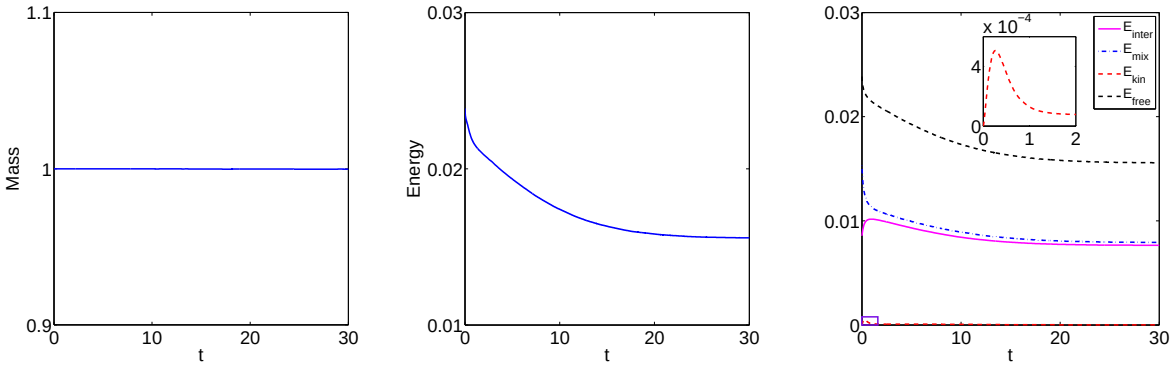

Figure 6: Evolution of normalized mass, discrete total energy and four energy terms.

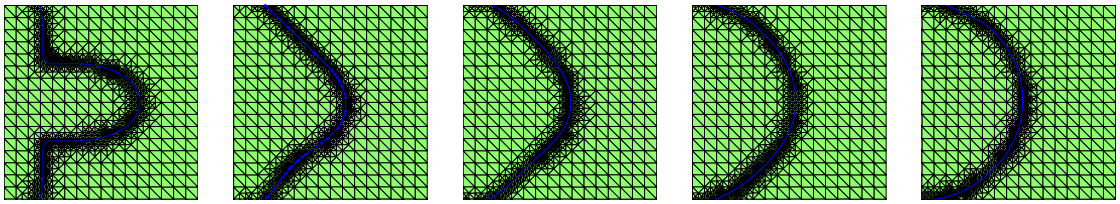

(a) $t = 0.0$ (b) $t = 1.5$ (c) $t = 2.0$ (d) $t = 3.0$ (e) $t = 5.0$

Figure 7: The enlarged adaptive mesh refinement on the restricted domain $[0.5, 1] \times [0.75, 1.25]$.

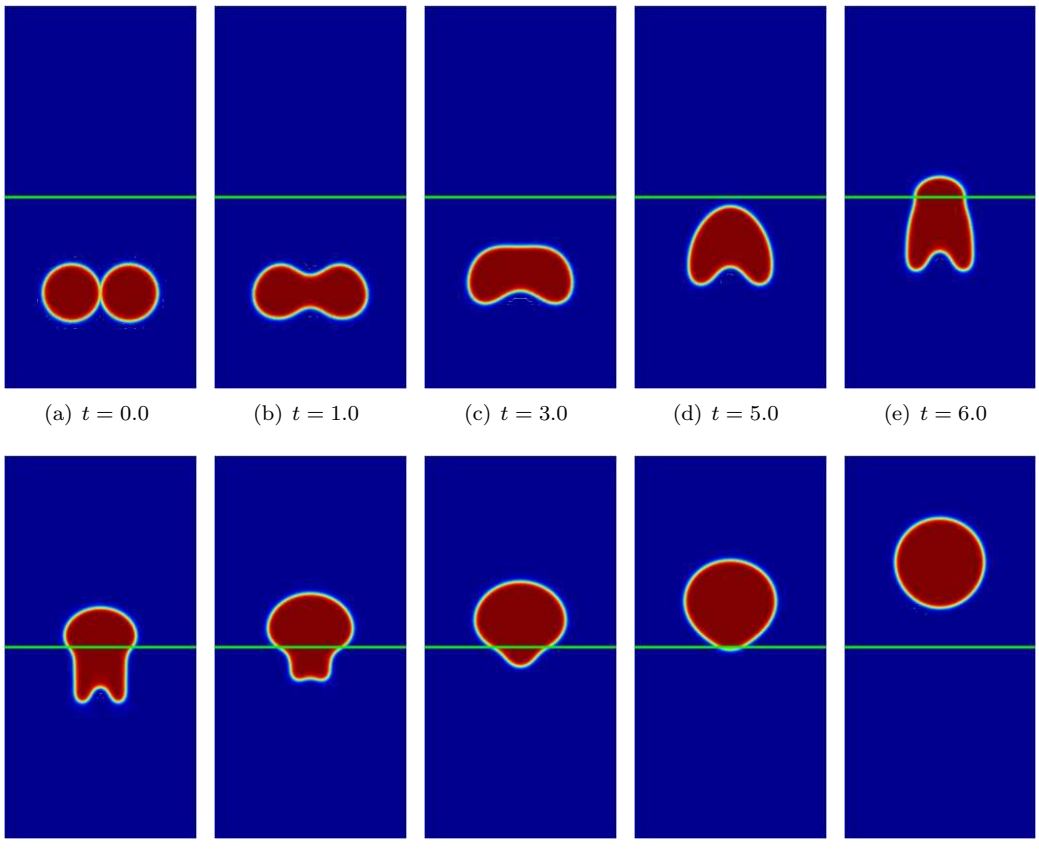

(a) $t = 0.0$ (b) $t = 1.0$ (c) $t = 3.0$ (d) $t = 5.0$ (e) $t = 6.0$

(f) $t = 7.0$ (g) $t = 8.0$ (h) $t = 9.0$ (i) $t = 11.0$ (j) $t = 15.0$

Figure 8: The evolution of horizontal rising bubbles in a heavier medium from left to right row by row.

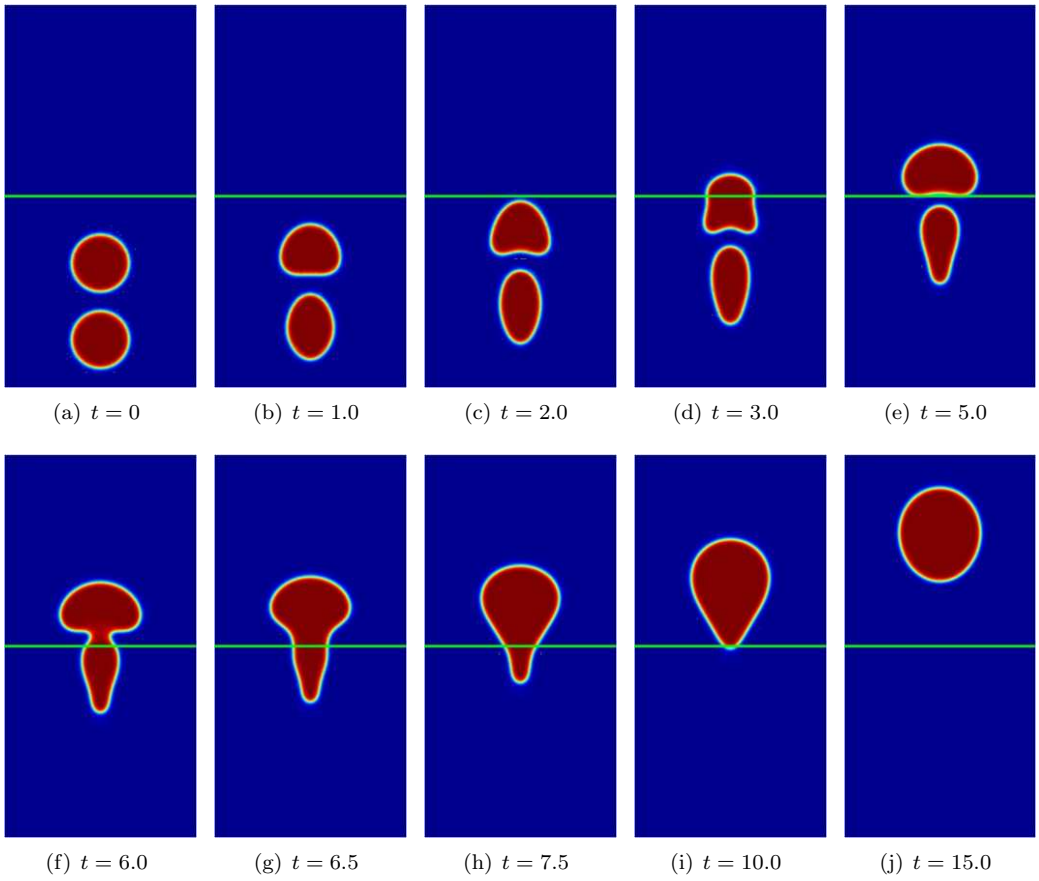

(a) $t = 0$ (b) $t = 1.0$ (c) $t = 2.0$ (d) $t = 3.0$ (e) $t = 5.0$

(f) $t = 6.0$ (g) $t = 6.5$ (h) $t = 7.5$ (i) $t = 10.0$ (j) $t = 15.0$

Figure 9: The evolution of vertical rising bubbles in a heavier medium from left to right row by row.

as the balance of computational efficiency and cost, the energy stability without time restriction, and the linear algebra system with constant coefficients only. The energy stability of the proposed method is rigorously proven. Moreover, we discuss the practical implementation details of proposed numerical scheme. Several numerical tests are also provided for the validation purpose.

Acknowledgement

The first author is partially supported by the NSFC grant 11901461. The second author is partially supported by the NSFC grant 11901372. The third author is partially supported by NSF grant DMS-2152609. The fourth author is partially supported by Hong Kong Special Administrative Region GRF grant 15302418.

References

[1] G. Akrivis, B. Li, and D. Li. Energy-decaying extrapolated RK-SAV methods for the Allen-Cahn and Cahn-Hilliard equations. *SIAM J. Sci. Comput.*, 41(6):A3703–A3727, 2019.

[2] P.F. Antonietti, L. Veiga, S. Scacchi, and M. Verani. A C^1 virtual element method for the Cahn-Hilliard equation with polygonal meshes. *SIAM J. Numer. Anal.*, 54(1):34–56, 2016.

[3] T. Arbogast and M. Gomez. A discretization and multigrid solver for a Darcy-Stokes system of three dimensional vuggy porous media. *Comput. Geosci.*, 13(3):331–348, 2009.

[4] T. Arbogast and H. L. Lehr. Homogenization of a Darcy-Stokes system modeling vuggy porous media. *Comput. Geosci.*, 10(3):291–302, 2006.

[5] M. G. Armentano and M. L. Stockdale. Approximations by mini mixed finite element for the Stokes-Darcy coupled problem on curved domains. *Int. J. Numer. Anal. Mod.*, 18:203–234, 2021.

[6] I. Babuška and G. N. Gatica. A residual-based a posteriori error estimator for the Stokes-Darcy coupled problem. *SIAM J. Numer. Anal.*, 48(2):498–523, 2010.

[7] L. Badea, M. Discacciati, and A. Quarteroni. Numerical analysis of the Navier-Stokes/Darcy coupling. *Numer. Math.*, 115(2):195–227, 2010.

[8] A. Baskaran, J. S. Lowengrub, C. Wang, and S. M. Wise. Convergence analysis of a second order convex splitting scheme for the modified phase field crystal equation. *SIAM J. Numer. Anal.*, 51(5):2851–2873, 2013.

[9] Y. Boubendir and S. Tlupova. Stokes-Darcy boundary integral solutions using preconditioners. *J. Comput. Phys.*, 228(23):8627–8641, 2009.

[10] Y. Boubendir and S. Tlupova. Domain decomposition methods for solving Stokes-Darcy problems with boundary integrals. *SIAM J. Sci. Comput.*, 35(1):B82–B106, 2013.

[11] M. Cai, M. Mu, and J. Xu. Numerical solution to a mixed Navier-Stokes/Darcy model by the two-grid approach. *SIAM J. Numer. Anal.*, 47(5):3325–3338, 2009.

[12] Y. Cao, M. Gunzburger, X.-M. He, and X. Wang. Robin-Robin domain decomposition methods for the steady Stokes-Darcy model with Beaver-Joseph interface condition. *Numer. Math.*, 117(4):601–629, 2011.

[13] Y. Cao, M. Gunzburger, X.-M. He, and X. Wang. Parallel, non-iterative, multi-physics domain decomposition methods for time-dependent Stokes-Darcy systems. *Math. Comp.*, 83(288):1617–1644, 2014.

[14] Y. Cao, M. Gunzburger, X. Hu, F. Hua, X. Wang, and W. Zhao. Finite element approximation for Stokes-Darcy flow with Beavers-Joseph interface conditions. *SIAM. J. Numer. Anal.*, 47(6):4239–4256, 2010.

[15] A. Çeşmelioğlu and B. Rivière. Existence of a weak solution for the fully coupled Navier-Stokes/Darcy-transport problem. *J. Differential Equations*, 252(7):4138–4175, 2012.

[16] J. Chen, S. Sun, and X. Wang. A numerical method for a model of two-phase flow in a coupled free flow and porous media system. *J. Comput. Phys.*, 268:1–16, 2014.

[17] W. Chen, M. Gunzburger, D. Sun, and X. Wang. Efficient and long-time accurate second-order methods for the Stokes-Darcy system. *SIAM J. Numer. Anal.*, 51(5):2563–2584, 2013.

[18] W. Chen, D. Han, and X. Wang. Uniquely solvable and energy stable decoupled numerical schemes for the Cahn-Hilliard-Stokes-Darcy system for two-phase flows in karstic geometry. *Numer. Math.*, 137(1):229–255, 2017.

[19] W. Chen, D. Han, X. Wang, and Y. Zhang. Uniquely solvable and energy stable decoupled numerical schemes for the Cahn-Hilliard-Navier-Stokes-Darcy-Boussinesq system. *J. Sci. Comput.*, 85(45):1–28, 2020.

[20] W. Chen, S. Wang, Y. Zhang, D. Han, C. Wang, and X. Wang. Error estimate of a decoupled numerical scheme for the Cahn-Hilliard-Stokes-Darcy system. *IMA Numer. Analysis*, 26(1-2):1–34, 2021.

[21] P. Chidyagwai, S. Ladenheim, and D. B. Szyld. Constraint preconditioning for the coupled Stokes-Darcy system. *SIAM J. Sci. Comput.*, 38(2):A668–A690, 2016.

[22] P. Chidyagwai and B. Rivière. On the solution of the coupled Navier-Stokes and Darcy equations. *Comput. Methods Appl. Mech. Engrg.*, 198(47-48):3806–3820, 2009.

[23] J.W. Choi, H.G. Lee, D. Jeong, and J. Kim. An unconditionally gradient stable numerical method for solving the Allen-Cahn equation. *Physica A*, 388:1791–1803, 2009.

[24] C. Collins, J. Shen, and R. Jari. An efficient, energy stable scheme for the Cahn-Hilliard-Brinkman system. *Comm. Comput. Phys.*, 13:929–957, 2013.

[25] V. DeCaria, T. Illiescu, W. Layton, M. McLaughlin, and M. Schneier. An artificial compression reduced order model. *SIAM J. Numer. Anal.*, 58:565–589, 2020.

[26] A. Diegel, X. Feng, and S. Wise. Analysis of a mixed finite element method for a Cahn-Hilliard-Darcy-Stokes system. *SIAM J. Numer. Anal.*, 53(1):127–152, 2015.

[27] M. Discacciati and L. Gerardo-Giorda. Optimized Schwarz methods for the Stokes-Darcy coupling. *IMA J. Numer. Anal.*, 38(4):1959–1983, 2018.

[28] M. Discacciati, P. Gervasio, A. Giacomini, and A. Quarteroni. The interface control domain decomposition method for Stokes-Darcy coupling. *SIAM J. Numer. Anal.*, 54(2):1039–1068, 2016.

[29] M. Discacciati, E. Miglio, and A. Quarteroni. Mathematical and numerical models for coupling surface and groundwater flows. *Appl. Numer. Math.*, 43(1-2):57–74, 2002.

[30] M. Discacciati and R. Oyarzúa. A conforming mixed finite element method for the Navier-Stokes/Darcy coupled problem. *Numer. Math.*, 135(2):571–606, 2017.

[31] M. Discacciati, A. Quarteroni, and A. Valli. Robin-Robin domain decomposition methods for the Stokes-Darcy coupling. *SIAM J. Numer. Anal.*, 45(3):1246–1268, 2007.

[32] C. C. Douglas, X. Hu, B. Bai, X.-M. He, M. Wei, and J. Hou. A data assimilation enabled model for coupling dual porosity flow with free flow. *17th International Symposium on Distributed Computing and Applications for Business Engineering and Science (DCABES), Wuxi, China, October 19-23, 2018*, DOI: 10.1109/DCABES.2018.00085.

[33] V. J. Ervin, E. W. Jenkins, and S. Sun. Coupled generalized nonlinear Stokes flow with flow through a porous medium. *SIAM J. Numer. Anal.*, 47(2):929–952, 2009.

[34] J. Fei, S. Xie, and C. Chen. A scalar suxiliary variable (SAV) and operator splitting compact finite difference method for peritectic phase field model. *Int. J. Numer. Anal. Model.*, 19:85–100, 2022.

[35] X.L. Feng, T. Tang, and J. Yang. Stabilized Crank-Nicolson/Adams-Bashforth schemes for phase field models. *East Asian J. Appl. Math.*, 3:59–80, 2013.

[36] Y. Gao, D. Han, X.-M. He, and U. Rüde. Unconditionally stable numerical methods for Cahn-Hilliard-Navier-Stokes-Darcy system with different densities and viscosities. *J. Comput. Phys.*, 454:#110968, 2022.

[37] Y. Gao, X.-M. He, L. Mei, and X. Yang. Decoupled, linear, and energy stable finite element method for the Cahn-Hilliard-Navier-Stokes-Darcy phase field model. *SIAM J. Sci. Comput.*, 40(1):B110–B137, 2018.

[38] Y. Gao, X.-M. He, and Y. Nie. Second-order, fully decoupled, linearized, and unconditionally stable SAV schemes for Cahn-Hilliard-Darcy system. *Numer. Methods Partial Differential Equations*, page doi: 10.1002/num.22829, 2022.

[39] V. Girault and B. Rivière. DG approximation of coupled Navier-Stokes and Darcy equations by Beaver-Joseph-Saffman interface condition. *SIAM J. Numer. Anal*, 47(3):2052–2089, 2009.

[40] V. Girault, D. Vassilev, and I. Yotov. Mortar multiscale finite element methods for Stokes-Darcy flows. *Numer. Math.*, 127(1):93–165, 2014.

[41] Z. Guan, C. Wang, and S.W. Wise. A convergent convex splitting scheme for the periodic nonlocal Cahn-Hilliard equation. *Numer. Math.*, 128:277–406, 2014.

[42] J. Guermond and P. Minev. High-order time stepping for the Navier-Stokes equations with minimal computational complexity. *J. Comput. Appl. Math.*, 310:92–103, 2017.

[43] M. Gunzburger, X.-M. He, and B. Li. On Ritz projection and multi-step backward differentiation schemes in decoupling the Stokes-Darcy model. *SIAM J. Numer. Anal.*, 56(1):397–427, 2018.

[44] C. Guo, J. Wang, M. Wei, X.-M. He, and B. Bai. Multi-stage fractured horizontal well numerical simulation and its application in tight shale reservoirs. *SPE-176714, SPE Russian Petroleum Technology Conference, Moscow, Russia, October 26-28, 2015*.

[45] D. Han, X.-M. He, Q. Wang, and Y. Wu. Existence and weak-strong uniqueness of solutions to the Cahn-Hilliard-Navier-Stokes-Darcy system in superposed free flow and porous media. *Nonlinear Anal.*, 211:#112411, 2021.

[46] D. Han, D. Sun, and X. Wang. Two-phase flows in karstic geometry. *Math. Methods Appl. Sci.*, 37(18):3048–3063, 2014.

[47] D. Han, D. Sun, and X. Wang. Existence and weak-strong uniqueness of solutions to the Cahn-Hilliard-Navier-Stokes-Darcy system in superposed free flow and porous media. *Nonlinear Anal.*, 211:112411, 2021.

[48] D. Han, Q. Wang, and X. Wang. Dynamic transitions and bifurcations for thermal convection in the superposed free flow and porous media. *Physica D*, 414:132687, 2020.

[49] D. Han, X. Wang, and H. Wu. Existence and uniqueness of global weak solutions to a Cahn-Hilliard-Stokes-Darcy system for two phase incompressible flows in karstic geometry. *J. Differential Equations*, 257(10):3887–3933, 2014.

[50] N. Hanspal, A. Waghode, V. Nassehi, and R. Wakeman. Numerical analysis of coupled Stokes/Darcy flow in industrial filtrations. *Transp. Porous Media*, 64:73–101, 2006.

[51] X.-M. He, N. Jiang, and C. Qiu. An artificial compressibility ensemble algorithm for a stochastic Stokes-Darcy model with random hydraulic conductivity and interface conditions. *Int. J. Numer. Methods Eng.*, pages 1–28, 2019.

[52] X.-M. He, J. Li, Y. Lin, and J. Ming. A domain decomposition method for the steady-state Navier-Stokes-Darcy model with Beavers-Joseph interface condition. *SIAM J. Sci. Comput.*, 37(5):S264–S290, 2015.

[53] P. Hessari. Pseudospectral least squares method for Stokes-Darcy equations. *SIAM J. Numer. Anal.*, 53(3):1195–1213, 2015.

[54] J. Hou, D. Hu, X.-M. He, and C. Qiu. Modeling and a Robin-type decoupled finite element method for dual-porosity-Navier-Stokes system with application to flows around multistage fractured horizontal wellbore. *Comput. Meth. Appl. Mech. Eng.*, 388:#114248, 2022.

[55] J. Hou, M. Qiu, X.-M. He, C. Guo, M. Wei, and B. Bai. A dual-porosity-Stokes model and finite element method for coupling dual-porosity flow and free flow. *SIAM J. Sci. Comput.*, 38(5):B710–B739, 2016.

[56] Q. Huang, X. Yang, and X.-M. He. Numerical approximations for a smectic-A liquid crystal flow model: first-order, linear, decoupled and energy stable schemes. *Discrete Contin. Dyn. Syst. Ser. B*, 23(6):2177–2192, 2018.

[57] N. Jiang, Y. Li, and H. Yang. An artificial compressibility Crank-Nicolson Leap-Frog method for the Stokes-Darcy model and application in ensemble simulations. *SIAM J. Numer. Anal.*, 59(1):401–428, 2021.

[58] G. Kanschat and B. Riviére. A strongly conservative finite element method for the coupling of Stokes and Darcy flow. *J. Comput. Phys.*, 229:5933–5943, 2010.

[59] D. Kay and R. Welford. Efficient numerical solution of Cahn-Hilliard-Navier-Stokes fluids in 2D. *SIAM J. Sci. Comput.*, 29(6):2241–2257, 2007.

[60] J. Kim, K. Kang, and J. Lowengrub. Conservative multigrid methods for Cahn-Hilliard fluids. *J. Comput. Phys.*, 193:511–543, 2004.

[61] J. Kou, S. Sun, and X. Wang. Linearly decoupled energy-stable numerical methods for multicomponent two-phase compressible flow. *SIAM J. Numer. Anal.*, 56(6):3219–3248, 2018.

[62] J. Kou, X. Wang, S. Du, and S. Sun. An energy stable linear numerical method for thermodynamically consistent modeling of two-phase incompressible flow in porous media. *J. Comput. Phys.*, 451:110854, 2022.

[63] P. Kumar, P. Luo, F. J. Gaspar, and C. W. Oosterlee. A multigrid multilevel Monte Carlo method for transport in the Darcy-Stokes system. *J. Comput. Phys.*, 371:382408, 2018.

[64] W. Layton, H. Tran, and C. Trenchea. Analysis of long time stability and errors of two partitioned methods for uncoupling evolutionary groundwater-surface water flows. *SIAM J. Numer. Anal.*, 51(1):248–272, 2013.

[65] W. J. Layton, F. Schieweck, and I. Yotov. Coupling fluid flow with porous media flow. *SIAM J. Numer. Anal.*, 40(6):2195–2218, 2002.

[66] R. Li, Y. Gao, J. Chen, L. Zhang, X.-M. He, and Z. Chen. Discontinuous finite volume element method for a coupled Navier-Stokes-Cahn-Hilliard phase field model. *Adv. Comput. Math.*, 46:#25, 2020.

[67] F. Lin, X.-M. He, and X. Wen. Fast, unconditionally energy stable large time stepping method for a new Allen-Cahn type square phase-field crystal model. *Appl. Math. Lett.*, 92:248–255, 2019.

[68] L. Lin, X. Liu, and S. Dong. A gPAV-based unconditionally energy-stable scheme for incompressible flows with outflow/open boundaries. *Comput. Methods Appl. Mech. Engrg.*, 365:112969, 2020.

[69] L. Lin, Z. Yang, and S. Dong. Numerical approximation of incompressible Navier-Stokes equations based on an auxiliary energy variable. *J. Comput. Phys.*, 388:1–22, 2019.

[70] K. Lipnikov, D. Vassilev, and I. Yotov. Discontinuous Galerkin and mimetic finite difference methods for coupled Stokes-Darcy flows on polygonal and polyhedral grids. *Numer. Math.*, 126(2):321–360, 2014.

[71] C. Liu and J. Shen. A phase field model for the mixture of two incompressible fluids and its approximation by a Fourier-spectral method. *Phys. D*, 179(3-4):211–228, 2003.

[72] J. Liu, L. Mu, and X. Ye. An adaptive discontinuous finite volume method for elliptic problems. *J. Comput. Appl. Math.*, 235(18):5422–5431, 2011.

[73] Y. Liu, Y. Boubendir, X.-M. He, and Y. He. New optimized Robin-Robin domain decomposition methods using Krylov solvers for the Stokes-Darcy system. *SIAM J. Sci. Comput.*, 44(4):B1068–B1095, 2022.

[74] J. Matusick and P. Zanbergen. Comparative study of groundwater vulnerability in a karst aquifer in central florida. *Geophy. Res. Abst.*, 9:1–1, 2007.

[75] M. Moraiti. On the quasistatic approximation in the Stokes-Darcy model of groundwater-surface water flows. *J. Math. Anal. Appl.*, 394(2):796–808, 2012.

[76] K. Mosthaf, K. Baber, B. Flemisch, R. Helmig, A. Leijnse, I. Rybak, and B. Wohlmuth. A coupling concept for two-phase compositional porous-medium and single-phase compositional free flow. *Water Resources Research*, 47(10):W10522, 2011.

[77] L. Mu and R. Jari. A posteriori error analysis for discontinuous finite volume methods of elliptic interface problems. *J. Comput. Appl. Math.*, 255:529–543, 2014.

[78] M. Mu and J. Xu. A two-grid method of a mixed Stokes-Darcy model for coupling fluid flow with porous

media flow. *SIAM J. Numer. Anal.*, 45(5):1801–1813, 2007.

[79] M. Mu and X. Zhu. Decoupled schemes for a non-stationary mixed Stokes-Darcy model. *Math. Comp.*, 79(270):707–731, 2010.

[80] A. Philippe and F. Pierre. Convergence results for the vector penalty-projection and two-step artificial compressibility methods. *Discrete Contin. Dyn. Syst. Ser. B*, 17:1383–1405, 2012.

[81] A. Prohl. On pressure approximation via projection methods for nonstationary incompressible Navier-Stokes equations. *SIAM J. Numer. Anal.*, 47(1):158–180, 2008.

[82] Z. Qiao, S. Sun, T. Zhang, and Y. Zhang. A new multi-component diffuse interface model with Peng-Robinson equation of state and its scalar auxiliary variable (SAV) approach. *Commun. Comput. Phys.*, 26(5):1597–1616, 2019.

[83] Y. Qin, C. Wang, and Z. Zhang. A positivity-preserving and convergent numerical scheme for the binary fluid-surfactant system. *Int. J. Numer. Anal. Model.*, 18:399–425, 2021.

[84] C. Qiu, X.-M. He, J. Li, and Y. Lin. A domain decomposition method for the time-dependent Navier-Stokes-Darcy model with Beavers-Joseph interface condition and defective boundary condition. *J. Comput. Phys.*, 411:#109400, 2020.

[85] B. Rivière and I. Yotov. Locally conservative coupling of Stokes and Darcy flows. *SIAM J. Numer. Anal.*, 42(5):1959–1977, 2005.

[86] I. Rybak and J. Magiera. A multiple-time-step technique for coupled free flow and porous medium systems. *J. Comput. Phys.*, 272:327–342, 2014.

[87] P. Saffman. On the boundary condition at the interface of a porous medium. *Stud. in Appl. Math.*, 1:77–84, 1971.

[88] L. Shan and H. Zheng. Partitioned time stepping method for fully evolutionary Stokes-Darcy flow with Beavers-Joseph interface conditions. *SIAM J. Numer. Anal.*, 51(2):813–839, 2013.

[89] J. Shen, C. Wang, X. Wang, and S.M. Wise. Second-order convex splitting schemes for gradient flows with Ehrlich-Schwoebel type energy: application to thin film epitaxy. *SIAM J. Numer. Anal.*, 50(1):105–125, 2012.

[90] J. Shen, J. Xu, and J. Yang. The scalar auxiliary variable (SAV) approach for gradient flows. *J. Comput. Phys.*, 353:407–416, 2018.

[91] J. Shen, J. Xu, and J. Yang. A new class of efficient and robust energy stable schemes for gradient flows. *SIAM Rev.*, 61(3):474–506, 2019.

[92] J. Shen and X. Yang. Numerical approximations of Allen-Cahn and Cahn-Hilliard equations. *Discrete Contin. Dyn. Syst.*, 28:1169–1691, 2010.

[93] J. Shen and X. Yang. Decoupled, energy stable schemes for phase-field models of two-phase incompressible flows. *SIAM J. Numer. Anal.*, 53(1):279–296, 2015.

[94] Y. Shi, K. Bao, and X-P Wang. 3D adaptive finite element method for a phase field model for the moving contact line problems. *Inverse Probl. Imaging*, 7(3):947–959, 2013.

[95] S. K. F. Stoter, P. Müller, L. Cicalese, M. Tuveri, D. Schillinger, and T. J. R. Hughes. A diffuse interface method for the Navier-Stokes/Darcy equations: perfusion profile for a patient-specific human liver based on MRI scans. *Comput. Methods Appl. Mech. Engrg.*, 321:70–102, 2017.

[96] M. Sussman, A.S. Almgren, J.B. Bell, P. Colella, and L.H. Howell. An adaptive level set approach for incompressible two-phase flows. *J. Comput. Phys.*, 148:81–124, 1999.

[97] D. Vassilev and I. Yotov. Coupling Stokes-Darcy flow with transport. *SIAM J. Sci. Comput.*, 31(5):3661–3684, 2009.

[98] W. Wang and C. Xu. Spectral methods based on new formulations for coupled Stokes and Darcy equations. *J. Comput. Phys.*, 257, part A:126–142, 2014.

[99] C. Xu, C. Chen, X. Yang, and X.-M. He. Numerical approximations for the hydrodynamics coupled binary surfactant phase field model: second order, linear, unconditionally energy stable schemes. *Commun. Math. Sci.*, 17(3):835–858, 2019.

[100] Y. Yan, W. Chen, C. Wang, and S.M. Wise. A second-order energy stable BDF numerical scheme for the Cahn-Hilliard equation. *Commun. Comput. Phys.*, 23(2):572–602, 2018.

[101] J. Yang, S. Mao, X.-M. He, X. Yang, and Y. He. A diffuse interface model and semi-implicit energy stable finite element method for two-phase magnetohydrodynamic flows. *Comput. Meth. Appl. Mech. Eng.*, 356:435–464, 2019.

[102] X. Yang. A novel fully-decoupled, second-order and energy stable numerical scheme of the conserved

Allen-Cahn type flow-coupled binary surfactant model. *Comput. Meth. Appl. Mech. Eng.*, 373:#113502, 2021.

[103] X. Yang. On a novel fully decoupled, second-order accurate energy stable numerical scheme for a binary fluid-surfactant phase-field model. *SIAM J. Sci. Comput.*, 43(2):B479–B507, 2021.

[104] X. Yang and D. Han. Linearly first- and second-order, unconditionally energy stable schemes for the phase field crystal equation. *J. Comput. Phys.*, 330:13–22, 2017.

[105] X. Yang and X.-M. He. A fully-discrete decoupled finite element method for the conserved AllenCahn type phase-field model of three-phase fluid flow system. *Comput. Meth. Appl. Mech. Eng.*, 389:#114376, 2022.

[106] X. Yang and X.-M. He. Numerical approximations of flow coupled binary phase field crystal system: fully discrete finite element scheme with second-order temporal accuracy and decoupling structure. *J. Comput. Phys.*, 467:#111448, 2022.

[107] X. Yang, J. Zhao, and X.-M. He. Linear, second order and unconditionally energy stable schemes for the viscous Cahn-Hilliard equation with hyperbolic relaxation using the invariant energy quadratization method. *J. Comput. Appl. Math.*, 343(1):80–97, 2018.

[108] Z. Yang and S. Dong. A roadmap for discretely energy-stable schemes for dissipative systems based on a generalized auxiliary variable with guaranteed positivity. *J. Comput. Phys.*, 404:109121, 2020.

[109] G. Zhang, X.-M. He, and X. Yang. Decoupled, linear, and unconditionally energy stable fully-discrete finite element numerical scheme for a two-phase ferrohydrodynamics model. *SIAM J. Sci. Comput.*, 43(1):B167–B193, 2021.

[110] G. Zhang, X.-M. He, and X. Yang. A fully decoupled linearized finite element method with second-order temporal accuracy and unconditional energy stability for incompressible MHD equations. *J. Comput. Phys.*, 448:#110752, 2022.

[111] H. Zhang, X. Yang, and J. Zhang. Stabilized invariant energy quadratization (S-IEQ) method for the molecular beam epitaxial model without slope section. *Int. J. Numer. Anal. Model.*, 18:642–655, 2021.

[112] Y. Zhang, J. Geng, J. Liu, B. Bai, X.-M. He, M. Wei, and W. Deng. Direct pore-level visualization and verification of in-situ oil-in-water pickering emulsification during polymeric nanogel flooding for EOR in a transparent three-dimensional micromodel. *Langmuir*, 37:13353–13364, 2021.

[113] Y. Zhang, C. Zhou, C. Qu, M. Wei, X.-M. He, and B. Bai. Fabrication and verification of a glass-silicon-glass micro-nanofluidic model for investigating multi-phase flow in unconventional dual-porosity porous media. *Lab Chip*, 19:4071–4082, 2019.

[114] B. Zhao, M. Zhang, and C. Liang. Global well-posedness for Navier-Stokes-Darcy equations with the free interface. *Int. J. Numer. Anal. Mod.*, 18:569–619, 2021.